



## OPEN ACCESS

## EDITED BY

Maoliang Zhang,  
Tianjin University, China

## REVIEWED BY

Jun Zhong,  
Tianjin University, China  
Zhihui Cheng,  
Lingnan Normal University, China

## \*CORRESPONDENCE

Ying Li,  
subduction6@hotmail.com  
Jianguo Du,  
jianguodu@hotmail.com

## SPECIALTY SECTION

This article was submitted to  
Geochemistry,  
a section of the journal  
Frontiers in Earth Science

RECEIVED 17 July 2022

ACCEPTED 14 November 2022

PUBLISHED 13 January 2023

## CITATION

Cui Y, Sun F, Liu L, Xie C, Li J, Chen Z, Li Y  
and Du J (2023), Contribution of deep-  
earth fluids to the geothermal system: A  
case study in the Arxan volcanic region,  
northeastern China.  
*Front. Earth Sci.* 10:996583.  
doi: 10.3389/feart.2022.996583

## COPYRIGHT

© 2023 Cui, Sun, Liu, Xie, Li, Chen, Li and  
Du. This is an open-access article  
distributed under the terms of the  
[Creative Commons Attribution License  
\(CC BY\)](https://creativecommons.org/licenses/by/4.0/). The use, distribution or  
reproduction in other forums is  
permitted, provided the original  
author(s) and the copyright owner(s) are  
credited and that the original  
publication in this journal is cited, in  
accordance with accepted academic  
practice. No use, distribution or  
reproduction is permitted which does  
not comply with these terms.

# Contribution of deep-earth fluids to the geothermal system: A case study in the Arxan volcanic region, northeastern China

Yueju Cui<sup>1</sup>, Fengxia Sun<sup>1</sup>, Lei Liu<sup>1</sup>, Chao Xie<sup>2</sup>, Jing Li<sup>3</sup>, Zhi Chen<sup>1</sup>,  
Ying Li<sup>1\*</sup> and Jianguo Du<sup>1\*</sup>

<sup>1</sup>United Laboratory of High-Pressure Physics and Earthquake Science, Key Laboratory of Earthquake Prediction, Institute of Earthquake Forecasting, CEA, Beijing, China, <sup>2</sup>The Second Monitoring and Application Center, CEA, Xi'an, China, <sup>3</sup>Institute of Disaster Prevention, Langfang, China

Investigations of the hot spring water and gas in the volcanic region are involved in assessing geothermal resources and understanding groundwater circulation, volcano, and earthquake activities. The origins of water and gas of the hot springs, lakes, rivers, and rain in the Arxan volcanic region (AVR), northeastern (NE) China, were investigated by conducting a field survey and geochemical analysis. The low electrical conductivity (40–835  $\mu\text{S}/\text{cm}$ ) and low total dissolved solids (TDS, 23.83–540.00 mg/L) of the water samples indicate that they are fresh water.  $\delta^{18}\text{O}$  and  $\delta\text{D}$  values of the water samples range from  $-4.1\%$  to  $-16.0\%$  and from  $-61.3\%$  to  $-119.9\%$ , respectively. Enrichment of heavy isotopes in the rainwater and the crater lake waters was caused by evaporation. The component  $\text{H}_2\text{O}$  of the water samples predominantly originated from the meteoric water, with less than 1 vol% contributed by deep-earth fluids. Ions in the rain sample were predominantly derived from sea salt and continental aerosol. Ions in the surface water samples had multiple origins (mineral dissolution, atmospheric, and anthropogenic sources). While the ions in the hot spring water were predominantly derived from both the dissolution of rocks and deep-earth fluids, the latter contributed 73%–87% of  $\text{Cl}^-$  and 86%–99% of  $\text{Na}^+$  to the hot spring waters. Gases from the hot springs were composed of more than 95%  $\text{N}_2$  and less than 5%  $\text{O}_2$  and Ar, with  $^3\text{He}/^4\text{He}$  ratios of 0.14–1.17  $R_A$  ( $R_A=1.4\times 10^{-6}$ ). Excess  $\text{N}_2$ , Ar, He, and  $\text{CO}_2$  of the hot springs were mainly derived from both the crust and upper mantle. About 3%–23% of the total He in the bubbling gases from the crater lake waters and hot springs is derived from the mantle, implying a supplement of heat energy from the mantle to the geothermal systems. Significantly, about 12% of the He dissolved in the Budonghe water is derived from the mantle, indicating that plenty of mantle-derived heat transported by deep-earth fluids keeps the river water from freezing. Our results indicate that Cl and Na ions and  $^3\text{He}/^4\text{He}$  ratio are the feasible geochemical indicators for source partitioning of geothermal fluids.

## KEYWORDS

geothermal system, Arxan volcanic region, hot spring water,  $^3\text{He}/^4\text{He}$  ratio, fluids

## 1 Introduction

The origins of geothermal fluids in the volcanic areas are involved in investigations of natural resources, environment, and hydrological cycle. Ion concentrations and isotope ratios of groundwater are the efficient indicators of water origin, circulation process of groundwater, geothermal potential, and volcanic activity (Giggenbach et al., 1993; Shaw et al., 2003; Taran, 2009, 2011; Benavente et al., 2016; Tardani et al., 2016; Rizzo et al., 2019). Therefore, geochemical observations of fluids can reveal the fluid origins, magmatic and seismic processes, and dynamic processes in the deep earth.

It is a major challenge in geoscience to decipher the complexity of fluids and minerals in the earth's interior. Sources of dissolved solids in groundwater can be divided into three categories: dissolution of minerals in circulation, deep-earth fluids, and atmospheric and anthropogenic sources. The deep-earth fluids, meaning waters, gases, and supercritical fluids that are derived from the deep crust and mantle, may be composited with different genetic types of fluids such as initial, magmatic, metamorphic, deep hydrothermal, and diagenetic fluids that usually mix into geothermal fluids. The origins of ions and gases can be traced by using concentrations and isotopic ratios of the chemical species and techniques of statistical analysis (Han et al., 2019; Li, 2020; Chen et al., 2021). A variable non-sea-salt contribution usually causes the slope to differ from the seawater ratio and the intercept to differ from zero (Keene et al., 1986).  $\text{Cl}^-$  and  $\text{Na}^+$  are the most reliable indicators for discriminating and partitioning sources of ions in the spring waters because they tend to exist in aqueous solution during water circulation, while other ions are partially fixed in secondary minerals.

Ion concentrations,  $\delta^{18}\text{O}$  and  $\delta\text{D}$ , of water have been widely used for investigating the origins of geothermal fluids. For instance, the high values of  $\delta^{18}\text{O}$ ,  $\delta\text{D}$ ,  $\delta^{13}\text{C}$ , and  $\text{Cl}^-$  concentrations of spring waters in Oita Plain, Japan, implied an origin of andesitic-magmatic steam or metamorphic water, while the low values of  $\delta\text{D}$  and Li and B concentrations of groundwater indicated meteoric water (Amita et al., 2005). Li et al. (2012) investigated the water vapor sources of meteoric water in NE China using  $\delta^{18}\text{O}$  and  $\delta\text{D}$  data. The hydrochemical data indicated that the main stream water of the Kherlen River in eastern Mongolia, neighboring to the west of the Arxan volcanic region (AVR), were recharged by meteoric water from the headwater region of more than 1,650 m altitude (Tsujimura et al., 2007).  $\delta^{18}\text{O}$  and  $\delta\text{D}$  values of the lake, river, and well waters in the Lake Hulun Basin neighboring to the north of the AVR indicated that the waters originated from meteoric water and suffered evident evaporation (Gao et al., 2018).

The concentrations of gaseous components, He/Ne,  $^4\text{He}/^{20}\text{Ne}$ ,  $\text{N}_2/\text{Ar}$ ,  $^3\text{He}/^4\text{He}$ ,  $\text{CO}_2/{}^3\text{He}$ , and  $\delta^{13}\text{C}$ , provide insight on the sources of the gaseous species in the geothermal and volcanic systems (Giggenbach et al., 1993; Shaw et al., 2003; Du et al.,

2005; Taran, 2009; 2011; Xu et al., 2013; Benavente et al., 2016; Rizzo et al., 2019; Bini et al., 2022), secondary processes of geothermal fluids (Zhang et al., 2016; Barry et al., 2020), volcanic and seismic activities (Chen et al., 2014; Zhou et al., 2015; Tardani et al., 2016), and contribution of volcanic gas to environment (Sun et al., 2020; Zhao et al., 2021). The regional variations in  $^3\text{He}/^4\text{He}$ ,  $\delta^{13}\text{C}$  of  $\text{CO}_2$ ,  $\delta^{15}\text{N}$ , and  $^{87}\text{Sr}/^{86}\text{Sr}$  values of hydrothermal fluids along an intra-arc fault system in the southern Volcanic Zone of the Chilean Andes indicated the geothermal gas was a mixture of mantle-derived gas and radiogenic gas in the crust (Tardani et al., 2016). The molecular and isotopic data of hot spring fluids and fumarolic gases in the Tateyama volcanic hydrothermal system in Japan (Seki et al., 2019), the Tengchong volcanic area (Du et al., 2005) and western Sichuan Province (Du et al., 2006) in southwestern China, and the Wudalianchi volcanic field (Du et al., 1999; Xu et al., 2013), Changbaishan volcano (CBV) (Wei et al., 2016), and the Songliao continental rift system (Zhao et al., 2019) in NE China indicated the gases were predominantly derived from the mantle and crustal sources.

The mantle worldwide and regionally appears heterogeneous. The crust and upper mantle in NE China are characterized by fluctuation of Moho depth, mantle uplift in the rift valley and geophysical and geochemical heterogeneities (Jia and Zhang, 2020). The crust thickness in the Greater Khingan Range orogenic belt ranges from 34.5 to 43.5 km, while it becomes 32.4–36.2 km in the Songliao Basin in the east (Li et al., 2014; Jia and Zhang, 2020). The statistic histogram of 279  $^3\text{He}/^4\text{He}$  ratios of mantle xenoliths in eastern China shows multiple peaks with a wider range from 0.1 to 12  $R_A$  (excluding eight individual data from 12.1 to 33  $R_A$ ;  $R_A$  is atmospheric  $^3\text{He}/^4\text{He} = 1.4 \times 10^{-6}$ ) (Cui et al., 2022). Isotopic ratios of noble gases in mantle xenoliths in the orogenic belt and rift valley indicate that the mantle in NE China is heterogeneous. Obviously, the geochemical characteristics of the mantle in NE China differ from those in the middle ocean ridge and volcanic arc (Sano and Marty, 1995; Shaw et al., 2003; Roulleau et al., 2015).

The previous investigations in AVR mainly involved geology, volcanology, geothermics and hydrology (Tang, 1984; Sun, 1999; Zhang, 2017; Gu et al., 2017; Chen et al., 2021). The hydrogeochemical investigations for 36 hot springs (defined as their temperatures being 5°C higher than the local annual atmospheric temperature) around the Hot Spring Museum, a natural museum established for tourism and spa in the Arxan city, suggested that the hot spring waters were chemically classified into Ca-Na-HCO<sub>3</sub>-SO<sub>4</sub>, Na-Ca-HCO<sub>3</sub>, and Na-HCO<sub>3</sub> (Gu et al., 2017; Zhang, 2017), and the residence time of high-temperature hot spring waters ranges from 70 a to 90 a, and that of low-temperature hot springs/shallow groundwater is about 10 a (Gu et al., 2017). Recently, the groundwater in the basalts of Arxan was considered exogenous water from the Tibetan Plateau based on the data of the water balance relationship and  $\delta^{18}\text{O}$  and  $\delta\text{D}$  values (Chen et al., 2021). Zhao et al. (2021) reported that

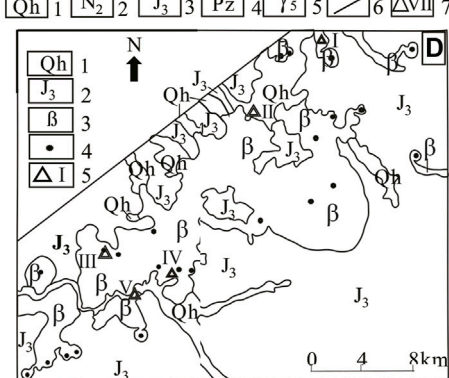
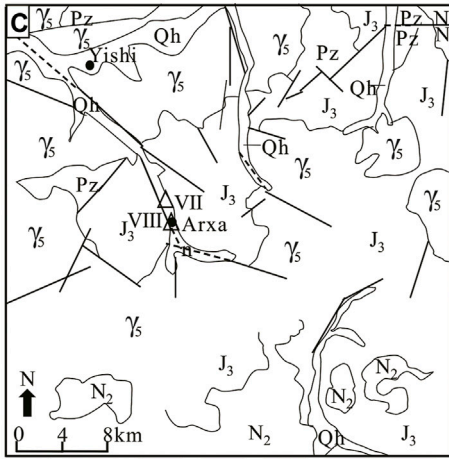
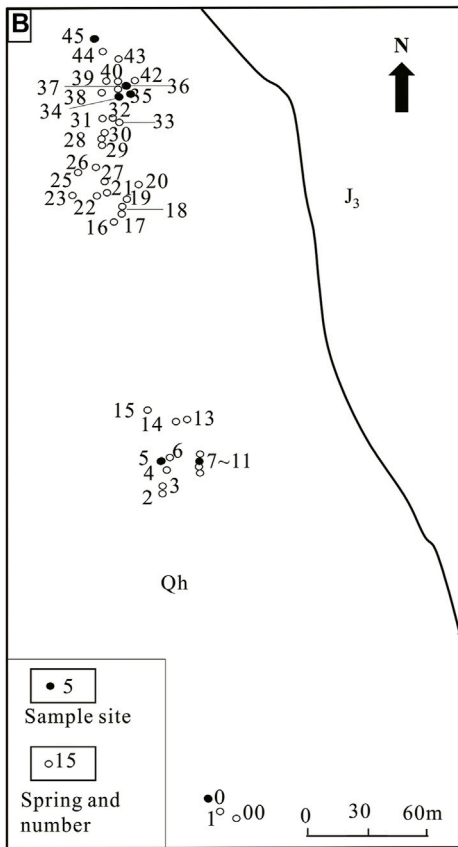
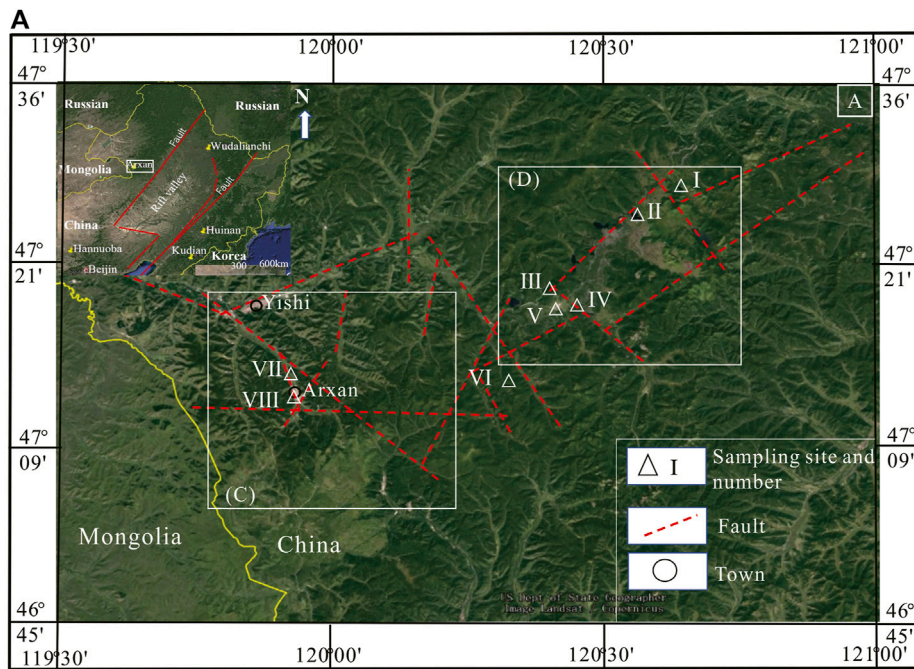


**FIGURE 1**  
**(A)** Topography of the study area and vicinity, showing main faults and the sampling sites (the image from Google Earth); the inset of the DEM image shows the location of the study area; sampling sites: I- Tuofengling; II- Dujuanhu; III- Tianchi; IV- Dichi; V- Budonghe; VI- Jinjianggou; VII- Wuliquan; VIII- the Hot Spring Museum. **(B)** Hot spring locations at the sampling site no. VIII, 45 springs occur in an area of 700 m long from north to south and 70 m wide from east to west (modified after Zhang (2017)). **(C)** Geological map of the Arxa volcanic region (square C in A); 1 - (Continued)

**FIGURE 1 (Continued)**

Holocene fluvial sediments; 2 - Neogene basalts, andesitic basalt, and andesite; 3 - Late Jurassic rhyolite and rhyolitic pyroclastic rocks; 4 - Paleozoic clastic rocks intercalated limestone; 5 - moyite; 6 - fault; 7 - sampling site and number (modified after Xie et al. (2011)). (D) Distribution of Holocene volcanism and sampling sites (square D in A), 1 - Holocene fluvial sediments; 2 - Late Jurassic rhyolite and rhyolitic pyroclastic rocks; 3 - Holocene alkali olivine basalts; 4 - Holocene crater; 5 - sampling site and number (modified after Fan et al. (2011)).

gases from two hot springs in the AVR were mainly composed of  $N_2$  with low  $^3He/^4He$  ratios (c. 0.1  $R_A$ ), high  $^4He/^{20}Ne$  ratios (150–380), and  $\delta^{13}C$  values of  $CO_2$  (-6.2% to -13.6%). They concluded that the spring gases were mainly derived from the crust. So far, the origins of hot spring fluids in the AVR remain debated. This paper aims at revealing the contribution of deep-earth fluids to the geothermal system in the AVR based on the molecular and ion concentrations and isotope compositions of the hot spring fluids.

## 2 Geological and hydrothermal setting

The AVR is famous for a lot of hot springs and Quaternary volcanoes. It is located at the west margin of northeastern (NE) China, where volcanic eruptions were very violent in the Cenozoic Era and produced more than 590 volcanoes and about 50,000  $km^2$  of exposed basalt (Liu et al., 2001). The altitudes in the AVR range from 900 m to 1,700 m (Figure 1A). The annual mean temperature is  $-2.5^\circ C$ , monthly averages of temperature range from  $10.5^\circ C$  to  $-31.2^\circ C$  with the lowest temperature of  $-45.7^\circ C$  recorded on 1<sup>st</sup> January 2001. Annual precipitation was 450 mm during 1951–2015, of which 80%–90% fell during June–September, whereas annual evaporation capacity is up to 1,116 mm (Gu et al., 2017; Chen et al., 2021).

The AVR tectonically belongs to the Greater Khingan Range orogenic belt that connects with the northern part of the continental rift valley on the east. There are mainly five groups of faults in the study area: NEE, NNE, NW, NNW, and EW trending faults. The NEE-trending Halaha River fault cuts the lithosphere with a length of ca. 500 km. The deep-cut faults provide two channels for Quaternary magma migration from the mantle: one displays a high temperature and fluid-enriched body approaching the depth of 10–12 km, and another has become cold above a depth of 30 km (Tang et al., 2005). The series of NNW-trending basement rifts deeply cut the crust, favoring the deep cycle of groundwater and the formation of hot springs.

Mesozoic igneous rocks are widely distributed in the AVR with a small area of Paleozoic clastic strata (Figure 1C). The Paleozoic strata are composed of Late Ordovician metamorphic clastic rocks and volcanic-sedimentary clastic rocks, Late Silurian metamorphic clastic rocks, and Early–Middle Devonian clastic rocks sandwiched with biogenic limestone. The Mesozoic strata

are mainly Late Jurassic rhyolitic lava and volcanic clastic rocks. The Cenozoic strata are Neogene clastic rocks and black basalts and Quaternary sediments (Fan et al., 2011; Xie et al., 2011).

Magmatic rocks in the study area are mainly the Early Indosinian and the Late-Middle Yanshanian porphyroid potassic granite, monzonitic granite, and moyite and Neogene and Quaternary basalts (Figures 1C, D). Alkaline basalts in the Greater Khingan Range are characterized by high MgO and Ni concentrations, high  $CaO/Al_2O_3$  ratios, enrichment of large lithophile elements and positive Nb-Ta anomalies, and moderately depleted Sr–Nb–Hf isotopic ratios. The basalts could be derived from the deep primary mantle, possibly from ancient primordial peridotite (Fan et al., 2003; Xue et al., 2019). Quaternary basalts in the AVR cover an area of ca. 100  $km^2$  and erupted from more than 54 craters in the Middle-Late Pleistocene and Holocene (Fan et al., 2011). The Yanshan Volcano is the youngest volcanic crater and has a radiocarbon age of 2,000 years (Bai et al., 2005).

Groundwaters in the study area can be classified into three types: (1) pore water in Quaternary fluvial sediments, discharging through river beds; (2) bedrock fissure water in Late Jurassic volcanic rocks, recharged by meteoric water and discharged through underflow to the river valley; and (3) vein-type fissure water in the fault zones (Chen et al., 2021). Surface waters include river water (the Halaha River and the Arshangole River), barrier lakes, and crater lakes. There are 45 hot springs around the Hot Spring Museum in Arxan town (Figure 1B), whose water temperatures range from 2 to  $40^\circ C$ . A unique phenomenon is that the distance between the low-temperature hot spring ( $2^\circ C$ ) and the high-temperature hot spring ( $40^\circ C$ ) is just 0.3 m, which could be caused by different amounts of deep-earth fluid recharge.

The heat flow in the Greater Khingan Range is  $40.2 \text{ mW/m}^2$ . The estimated Moho heat flow is  $33.2 \text{ mW/m}^2$  (Sun, 1999). Though the regional heat flow is low, three geothermal fields have been found in the AVR (Qi et al., 2012). One is the Jinjiangguo (JJG) Valley geothermal field, which is composed of two geothermal zones controlled by the NE and NNW trending faults in granite and characterized by lower resistance. The geothermal water age was dated as  $8,150 \pm 90 \text{ a}$  (Qi et al., 2012). The second one is the Yinjianggou Valley (YJG) geothermal field, which is controlled by a NNW-trending fault. The third one is the Wuliqiao geothermal field, which is controlled by EW- and NNW-trending faults (Qi et al., 2012). The thermal energy is derived from the mantle (magma) and radiogenic heat in the crust (Qi et al., 2012). The heat energy of the hot springs around the Hot Spring Museum could be mainly derived from radiogenic heat in the crust (Sun, 1999).

TABLE 1 Ion concentrations and isotopic ratios of the water samples from the Arxan volcanic region.

ID	Location	Type	T (°C)	EC (μS/cm)	PH	mg/L											TDS	i.b %	‰V-SMOW		Water type	‰	
						Li <sup>+</sup>	Na <sup>+</sup>	NH <sub>4</sub> <sup>+</sup>	K <sup>+</sup>	Mg <sup>2+</sup>	Ca <sup>2+</sup>	F <sup>-</sup>	Cl <sup>-</sup>	NO <sub>3</sub> <sup>-</sup>	SO <sub>4</sub> <sup>2-</sup>	HCO <sub>3</sub> <sup>-</sup>			δ <sup>18</sup> O	δD		Na*	Cl*
AW-0	VO	Rain	20.0	41.3	7.74	0.01	2.0	0.5	0.6	0.4	5.9	0.1	0.5	3.7	3.2	19.8	26.9	-0.32	-8.5	-94.4	Ca-HCO <sub>3</sub>	98	85
AW-1	Dichi	Lake	19.2	95.8	7.66		7.9	0.4	1.8	3.5	10.2	0.4	1.4	0.9	6.9	56.2	61.4	-0.32	-13.1	-103.5	Na-HCO <sub>3</sub>		
AW-2	TFL Tianchi	Lake	18.6	40.0	7.31		2.7	0.4	0.5	2.1	4.2	0.1	0.5	0.6	2.0	28.1	27.2	-0.34	-5.1	-61.3	Na-Ca-HCO <sub>3</sub>		
AW-3	Dujuanhu	Lake	19.8	51.4	7.29		3.3	0.5	0.3	2.0	7.4	2.4	0.4	3.0	5.8	28.1	39.2	-0.33	-10.9	-87.6	Ca-Mg-HCO <sub>3</sub>		
AW-4	Tianchi	Lake	21.8	40.3	6.92		2.4	0.3	0.2	2.2	3.7	0.8	0.7	1.3	1.2	22.1	23.8	-0.30	-4.1	-61.4	Ca-Mg-HCO <sub>3</sub>		
AW-5	Budonghe	River	7.5	90.8	7.68	0.01	6.2	0.5	1.1	3.7	11.2	0.2	0.03	0.1	7.2	58.3	59.2	-0.32	-13.4	-106.2	Ca-Mg-HCO <sub>3</sub>		
AW-6	JJG	HS	37.5	614.0	7.59	0.04	120.6	3.0	3.1	1.4	20.4	14.6	20.6	0.0	151.3	152.7	411.3	-0.48	-15.1	-111.7	Na-HCO <sub>3</sub>		
AW-7	JJG	Well	19.9	577.0	7.58	0.04	121.3	3.5	3.2	1.5	22.4	9.8	18.1	0.1	137.9	152.7	394.0	-0.44	-15.0	-111.4	Na-HCO <sub>3</sub>	98	83
AW-8	JJG	HS	27.4	471.0	7.79	0.03	81.7	3.6	2.7	2.9	30.4	6.3	12.8	1.8	101.4	158.7	323.9	-0.42	-14.6	-111.1	Na-HCO <sub>3</sub>	96	76
AW-9	Wuliquan	HS	3.5	391.0	7.76	0.02	53.6	3.3	2.4	5.9	38.7	1.8	22.1	30.5	39.2	156.7	275.9	-0.32	-16.0	-118.4	Na-HCO <sub>3</sub>	94	86
AW-10	HSM no. 34	HS	36.4	644.0	8.18	0.07	169.6	4.5	4.1	2.7	12.0	10.5	16.1	8.4	69.4	321.4	458.0	-0.41	-16.0	-116.8	Na-HCO <sub>3</sub>	98	81
AW-11	HSM no. 35	HS	25.1	691.0	7.77	0.05	155.0	4.4	4.3	2.7	25.1	7.6	17.2	20.3	69.0	372.5	491.7	-0.43	-15.8	-115.0	Na-HCO <sub>3</sub>	98	83
AW-12	HSM no. 36	HS	24.3	761.0	8.05	0.06	182.1	3.9	4.4	1.7	17.2	8.7	19.5	20.8	82.7	398.5	540.0	-0.46	-15.3	-113.8	Na-HCO <sub>3</sub>	98	85
AW-13	HSM no. 45	HS	23.9	835.0	7.97	0.08	219.1	4.1	4.2	1.1	15.0	11.0	23.6	26.8	114.7	385.5	612.3	-0.45	-15.6	-114.4	Na-HCO <sub>3</sub>	99	87
AW-14	HSM no. 7	HS	17.0	179.8	7.83	0.01	35.4	3.3	2.1	1.9	8.4	1.8	3.8	5.3	20.1	108.3	136.2	-0.44	-15.7	-119.9	Na-HCO <sub>3</sub>	92	
AW-15	HSM no. 5	HS	16.6	211.3	7.71		21.8	2.5	1.5	4.1	24.8	1.4	11.2	21.1	22.2	80.1	150.5	-0.31	-15.4	-118.3	Na-HCO <sub>3</sub>	86	73
AW-16	HSM no. 3	HS	17.0	408.0	7.97	0.03	78.3	4.4	3.2	3.2	22.6	3.3	15.8	35.5	46.4	175.4	300.3	-0.40	-15.3	-116.2	Na-HCO <sub>3</sub>	96	81

VO - the volcano observatory; HS - hot spring; TFL - Tuofengling; JJG - Jinjianguo; empty cell is less than the detection limit; Na\* and Cl\*- calculated percentages of Na<sup>+</sup> and Cl<sup>-</sup> derived from deep-earth fluids.

### 3 Sample and method

The water and gas samples were collected from the AVR in August 2010 (Figure 1). The field measurements of water temperature, electrical conductivity (EC), and pH were conducted with the portable instruments. The samples for hydrochemical analysis were collected with the 250-ml plastic bottles, and for stable isotopic analysis of H and O with the 2-ml plastic bottles. The gas samples were collected by the gas drainage method in 1,000-ml glass bottles and sealed with rubber caps (Du et al., 2006). Totally, 17 water samples were collected from the springs, crater lakes, river, and rain, and eight gas samples were collected including seven bubbling gases and one dissolved gas in the water of the Budonghe River (at the sampling site V in Figure 1). The rain sample is the thundershower water dropped down from the building rooftop after filtering dust particles.

Concentrations of  $\text{Li}^+$ ,  $\text{Na}^+$ ,  $\text{NH}_4^+$ ,  $\text{K}^+$ ,  $\text{Ca}^{2+}$ ,  $\text{Mg}^{2+}$ ,  $\text{F}^-$ ,  $\text{Cl}^-$ ,  $\text{NO}_3^-$ , and  $\text{SO}_4^{2-}$  were measured with a Dionex ICS-900 ion chromatography system with the standard configuration (reproducibility within  $\pm 2\%$ ). The  $\text{HCO}_3^-$  concentrations were measured by the standard titration procedures with a ZDJ-100 potentiometric titrator (reproducibility within  $\pm 2\%$ ) (Chen et al., 2014). Ion charge balance errors (I.B.) of the hydrochemical data are less than  $\pm 5\%$ . The total dissolved solid (TDS) value was calculated by,  $\sum X_i - (\text{HCO}_3^-)/2$ , subtracting total ion concentration minus the half of  $\text{HCO}_3^-$  concentration (Table 1). Stable isotope ratios of H and O were measured with a MAT 253 mass spectrometer at Hehai University, and the  $\delta^{18}\text{O}$  and  $\delta\text{D}$  values were reported referring to the V-SMOW standard with errors of 0.1% and 2‰, respectively (Chen et al., 2021).

The  $\text{N}_2$ ,  $\text{O}_2$ , Ar,  $\text{CO}_2$ ,  $\text{CH}_4$ , and He concentrations of the gas sample were analyzed with a Finnigan MAT-271 mass spectrometer, with a precision of  $\pm 0.1\%$ . Helium and neon isotope compositions of the gas samples were measured with an MM5400 mass spectrometer at the Laboratory of Gas Geochemistry, the Institute of Geology and Geophysics, the Chinese Academy of Sciences.  $\delta^{13}\text{C}$  values of  $\text{CH}_4$  and  $\text{CO}_2$  were measured with the GC-IRMS analytical system, a gas chromatography (Agilent 6890)-stable isotope ratio mass spectrometer, and the values of  $\text{C}^{13}\text{C}$  are reported relative to PDB in per mill with an error of  $\pm 0.5\%$  (Li et al., 2007; Zhou et al., 2015). It is worthy of mention that the He concentration and  $^4\text{He}/^{20}\text{Ne}$  ratios of dissolved gas in the Budonghe water are double of atmospheric values. The  $^3\text{He}/^4\text{He}$  ratio was less than the atmospheric ratio, which indicates the sample was not contaminated by air during sampling and analysis.

### 4 Results

The temperatures of the hot spring waters are in a range of 2.3°C–37.5°C. The water temperatures of the springs no. 5 at the Hot Spring Museum and Wuliquan (at 2.5 km northwest Arxan town) are lower than those of Budonghe water (7.5°C). The water

samples have low electric conductivity (40–835  $\mu\text{S}/\text{cm}$ ) and low TDS (23.83–540.00 mg/L). TDS values of the surface (river and lake) waters are lower than those of the hot spring waters. Abundance of the majority cations and anions is generally in the order of  $\text{Na}^+ > \text{Ca}^{2+} > \text{Mg}^{2+} > \text{K}^+ > \text{NH}_4^+$  and  $\text{HCO}_3^- > \text{SO}_4^{2-} > \text{Cl}^-$ ,  $\text{NO}_3^- > \text{F}^-$ , respectively.  $\delta^{18}\text{O}$  and  $\delta\text{D}$  values of the water samples range from -4.1% to -16.0% and -61.3% to -119.9%, respectively. The lake waters are more enriched in heavy isotopes ( $^{18}\text{O}$  and D) than the hot spring waters (Table 1).

The molecular and isotope compositions of the gas samples are listed in Table 2 including some published data (Zhao et al., 2021) in the AVR for comparison. The  $\text{N}_2$  concentrations of the gas samples from the AVR are more than 95%, and others together are less than 5%.  $^3\text{He}/^4\text{He}$  ratios are in a range of  $0.20 \times 10^{-7} \sim 1.64 \times 10^{-6}$ .  $^4\text{He}/^{20}\text{Ne}$  ratios of the surface waters are approximately equal to the atmospheric value (0.32), but those of hot spring waters are much higher than the atmospheric value.  $\text{CO}_2$  concentrations are lower (0.13%–0.41%) and  $\delta^{13}\text{C}$  of  $\text{CO}_2$  from -22.3% to -6.2%.  $\delta^{13}\text{C}$  of methane ( $\text{C}_1$ ) from Tianchi is -51.5%, indicating the biogenic origin of  $\text{C}_1$ , but  $\delta^{13}\text{C}$  of  $\text{C}_1$  from the geothermal well in JJG is 1.4‰, hinting at an abiogenic origin.  $^{21}\text{Ne}/^{22}\text{Ne}$  and  $^{20}\text{Ne}/^{22}\text{Ne}$  ratios are approximated by the atmospheric values (0.029 and 9.78, respectively).

## 5 Discussion

### 5.1 Origins of the water components

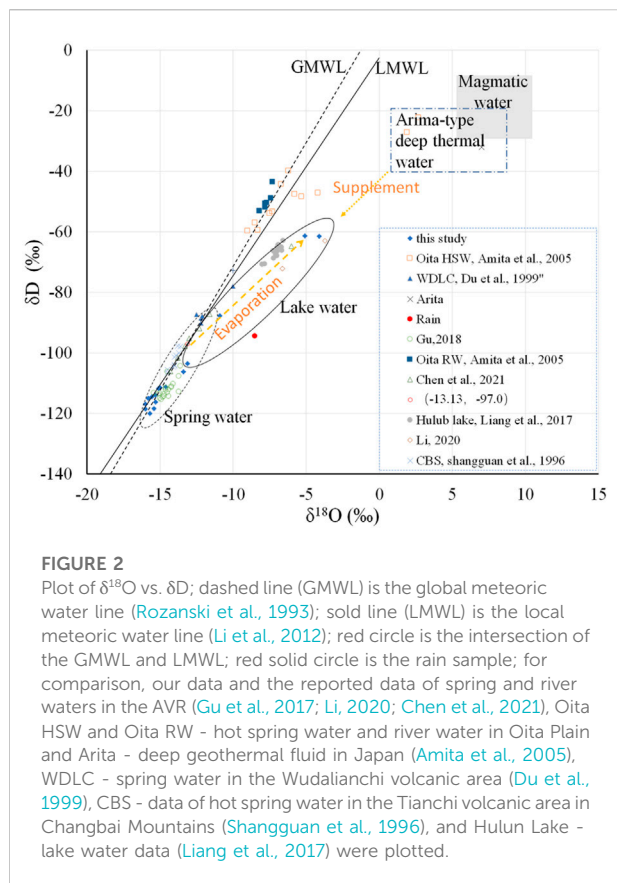
#### 5.1.1 Isotopic compositions of hydrogen and oxygen

Most  $\delta^{18}\text{O}$  and  $\delta\text{D}$  values of the water samples are scattered nearby the global meteoric water line (GMWL),  $\delta\text{D} = 8.17\delta^{18}\text{O} + 10.35$ , (Rozanski et al., 1993) and the local meteoritic water line (LMWL) in NE China ( $\delta\text{D} = 7.20\delta^{18}\text{O} - 2.39$ , Li et al., 2012), but some shift far to the right side of the lines (Figure 2). The coordinates (-13.1% and -97.0%) of the intersection between the GMWL and LMWL can be regarded as the mean value of the initial source water (Han et al., 2019). The slope and intercept of the LMWL are smaller than those of the GMWL, indicating evaporation effect and multiple origins of waters (Tsujiyama et al., 2007; Li et al., 2012; Han et al., 2019). The isotopic data of the spring and river waters in the AVR, the spring waters in Wudalianchi (Du et al., 1999) and CBV (Shangquan et al., 1996), and the river waters in Oita Plain, Japan (Amita et al., 2005), are scattered along the GMWL, indicating that those waters are mainly derived from the Pacific Ocean. This conclusion is supported by the fact that the meteoric water in northeastern China is mainly derived from the Pacific Ocean during the summer monsoon season. The wide ranges of  $\delta^{18}\text{O}$  and  $\delta\text{D}$  values (Table 1) indicated that the different kinds of waters experienced different processes of isotopic fractionation.

TABLE 2 Molecular and isotope compositions of gases from the springs and lakes in the Arxan volcanic region.

Location	T °C	Sampling date	N <sub>2</sub>	O <sub>2</sub>	Ar	CO <sub>2</sub>	N*	Ar*	CH <sub>4</sub> ×10 <sup>-6</sup>	He ×10 <sup>-6</sup>	<sup>3</sup> He/ <sup>4</sup> He ×10 <sup>-6</sup>	<sup>3</sup> He/ <sup>4</sup> He	<sup>3</sup> He/ <sup>4</sup> He*	δ <sup>13</sup> C <sub>CO2</sub> ‰PDB	δ <sup>15</sup> N ‰ Air	<sup>20</sup> Ne/ <sup>22</sup> Ne	<sup>21</sup> Ne/ <sup>22</sup> Ne	<sup>4</sup> He/ <sup>20</sup> Ne ×10 <sup>3</sup>	N <sub>2</sub> / Ne	He (%)			
																				Atm			
Dichi	19.2	2010.08	95.55	2.15	1.86	0.34	91.65	1.76	98.0	6.0	1.41	1.01	1.02	-15.9	1.9	9.96	0.028	0.44	0.12	56	21	23	5
TFL Tianchi	18.6	2010.08								7.0	1.64	1.17	1.53			11.50	0.028	0.36		68	23	9	6
Tianchi	21.8	2010.08								4.0	1.12	0.80	0.27			9.77	0.025	0.34		73	3	24	1
Budonghe	7.5	2010.08								9.0	0.92	0.66	0.44	-18.4		10.06	0.027	0.62		39	12	48	3
JJG HS	37.5	2010.08								8212.0	0.29	0.21	0.21			9.72	0.026	385.30		0	9	91	2
JJG HS	19.9	2010.08	97.19	0.56	1.73	0.41	96.17	1.70	12.0	7338.0	0.30	0.22	0.22	-21.0		10.05	0.023	293.45	0.12	0	9	90	2
HSM no. 34	27.4	2010.08								6469.0	0.23	0.16	0.16	-18.2		10.54	0.026	257.79		0	7	93	2
HSM no. 0	3.5	2010.08								1.0	0.27	0.19	0.16	-22.3		9.80	0.025	7.03		3	7	90	2
JJG HS <sup>a</sup>	36.6	2018.09	96.70	1.45	1.45	0.18	94.07	1.38		3191	0.238	0.17	0.17	-6.2				334	0.30	0	7	93	2
JJG HS <sup>a</sup>	36.6	2018.09	95.83	1.83	1.14	0.26	92.51	1.05		2840	0.196	0.14	0.14	-8.7	1.3			152	0.34	0	6	94	1
JJG HS <sup>a</sup>	24.8	2018.09	96.60	1.93	1.19	0.14	93.10	1.10		1457	0.252	0.18	0.18	-10.7	1.6			306	0.66	0	8	92	2
JJG HS <sup>a</sup>	24.8	2018.09	96.53	2.01	1.18	0.12	92.88	1.08		1585	0.224	0.16	0.16	-13.7	1.7			384	0.61	0	7	93	2
JJG HS <sup>a</sup>	24.8	2018.09	96.56	1.97	1.19	0.13	92.99	1.09															
Air			78.08	20.95	0.93	0.04			1.80	5.24		1.4		-7	0	9.78	0.029	0.318	149.3				
ASW <sup>b</sup>			17.070	9.409	0.459													0.245					

a. after [Zhao et al. \(2021\)](#); b. gas concentration in air-saturated water (ASW) at 3 °C (ml/L) after [Weiss \(1970, 1971\)](#); empty cell is no data; N\*: excess N<sub>2</sub> corrected by the N<sub>2</sub>/O<sub>2</sub> ratio of ASW at 3 °C, N\* = N<sub>2</sub> - 1.814 O<sub>2</sub>; Ar\*: excess Ar corrected by the O<sub>2</sub>/Ar ratio of ASW at 3 °C, Ar\* = Ar - O<sub>2</sub>/20.5; <sup>3</sup>He/<sup>4</sup>He\*: ASW-corrected <sup>3</sup>He/<sup>4</sup>He ratio; Atm: percentage of atmospheric He in the total He of the hot spring gases; LM: the estimated percentage of mantle-derived He considering the HNB <sup>3</sup>He/<sup>4</sup>He ratio (2.1 R<sub>A</sub>) as the local mantle helium source; CR: percentage of crustal He; PM: the estimated percentage of mantle helium considering the MORB <sup>3</sup>He/<sup>4</sup>He ratio (8 R<sub>A</sub>) as the primary mantle source; others are same as in [Table 1](#).



$\delta^{18}\text{O}$  and  $\delta\text{D}$  values of the rain sample (AW-0) are scattered far from the LMWL (Figure 2). The heavier isotope compositions of the rain sample are concordant with those of rain in the Hulun Lake Basin (Liang et al., 2017), NE China (Li et al., 2012), and eastern Mongolia in summer (Tsujimura et al., 2007). Therefore, the heavier isotope compositions of the rain sample can be attributed to the seasonal isotopic variations of meteoric water. In the east-west extended climate zone from the Greater Khingan Range to the Mongolia Plateau, the isotopic compositions of H and O in meteoric water are characterized by obviously seasonal variation of more negative values in winter than those in summer (Tsujimura et al., 2007; Gao et al., 2018; Li, 2020).

The surface water samples (AW-1–AW-5) were relatively enriched in heavy isotopes but depleted in the TDS (<62 mg/L) (Table 1; Figure 2).  $\delta^{18}\text{O}$  and  $\delta\text{D}$  values of water samples from the Dichi (a crater lake of the maar volcano) and Budonghe are similar. The water samples from the Tianchi and Tuofengling (TFL) Tianchi, two crater lakes on the volcanic cones, are more enriched in heavy isotopes. The Dujuehu is a barrier lake, whose water is more enriched in D (Table 1). The d-excess ( $\delta\text{D}-8.17\delta^{18}\text{O}$ ) of the lake water samples is much lower than that of the LMWL (Figure 2). Such isotopic shifts can be mainly attributed to the evaporation of raindrops and lake water caused by higher evaporation capacities.

$\delta\text{D}$  and  $\delta^{18}\text{O}$  values of seven water samples collected at the Hot Spring Museum and three water samples from the hot springs in JJG and previous results (Sun, 1999; Gu et al., 2017; Li, 2020; Chen et al., 2021) scattered nearby the LMWL, which indicates that the hot spring waters in the AVR mainly originated from meteoric water (Figure 2). The depletion of heavy isotopes in the hot spring waters can be explained by the air temperature effect because the isotopic fractionations of O and H in meteoric water are mainly related to the thermal dynamics of water vapor condensation. Both  $\delta\text{D}$  and  $\delta^{18}\text{O}$  values of meteoric water and surface air temperature in north China (latitude higher than  $36^\circ\text{N}$ ) have positive correlation.  $\delta^{18}\text{O}/\text{T}$  gradient was  $0.52\text{‰}/^\circ\text{C}$ , and  $\delta\text{D}/\text{T}$  gradient was  $4.27\text{‰}/^\circ\text{C}$  (Zhang et al., 2008). Let us take the Hailun station in the Songliao Basin ( $47.45^\circ\text{N}$ ,  $126.93^\circ\text{E}$ , an altitude of 236 m, an annual mean of  $5.5^\circ\text{C}$ , and 480 km to NE Arxan) of the Chinese Network of Isotopes in Precipitation as a reference, the mean values of  $\delta^{18}\text{O}$  and  $\delta\text{D}$  of meteoric water are  $-12.5\text{‰}$  and  $-92.2\text{‰}$  at the Hailun station (Liu et al., 2014). The temperature difference of  $8.0^\circ\text{C}$  between Hailun and Arxan results in the  $\delta^{18}\text{O}$  and  $\delta\text{D}$  differences of 4.2% and 34.2%, respectively. Consequently, the  $\delta^{18}\text{O}$  and  $\delta\text{D}$  values of meteoric water in Arxan are estimated to be, respectively,  $-16.7\text{‰}$  and  $-126.4\text{‰}$ . In reverse, the isotopic coordinates of intersection between the GMWL and LMWL, regarding the mean value of recharge source water, minus the O and H isotope fractionation caused by decreasing temperature, are equal to  $-17.3\text{‰}$  and  $121.2\text{‰}$ , respectively, which are concordant with the isotopic ratios of the spring waters in the AVR (Table 1).

### 5.1.2 Ions in the waters

The TDS values of all water samples range from 23.83 to 540.00 mg/L, indicating the waters are fresh. The waters can be chemically classified into four groups, namely,  $\text{Na}-\text{HCO}_3$ ,  $\text{Ca}-\text{HCO}_3$ ,  $\text{Ca}-\text{Mg}-\text{HCO}_3$ , and  $\text{Na}-\text{Ca}-\text{HCO}_3$  by Sokolov's method (Sokolov, 1966). All the spring water samples are  $\text{Na}-\text{HCO}_3$  type, four samples from the crater lakes are  $\text{Ca}-\text{Mg}-\text{HCO}_3$ ,  $\text{Na}-\text{Ca}-\text{HCO}_3$ ,  $\text{Ca}-\text{HCO}_3$ , and  $\text{Na}-\text{HCO}_3$ , one from the Budonghe River is  $\text{Ca}-\text{Mg}-\text{HCO}_3$ , and a rain sample is  $\text{Ca}-\text{HCO}_3$  type (Table 1).

The results of the correlation analysis for the hydrochemical parameters show that there is a strong positive correlation ( $r > 0.8$ , Table 3) between TDS and  $\text{Li}^+$ ,  $\text{Na}^+$ ,  $\text{K}^+$ ,  $\text{NH}_4^+$ ,  $\text{HCO}_3^-$ ,  $\text{Cl}^-$ ,  $\text{F}^-$ , and  $\text{SO}_4^{2-}$ , indicating that the TDS of the water samples is mainly controlled by deep-earth fluids and the dissolution of rocks. This is supported by the higher  $\text{Na}^+$  and  $\text{Cl}^-$  concentrations, TDS, and temperatures of the hot spring waters and the residence time (Gu et al., 2017). Cui et al. (2022) reported that 85% of the TDS of continental meteoric water was composed of  $\text{SO}_4^{2-}$ ,  $\text{Ca}^{2+}$ ,  $\text{NO}_3^-$ ,  $\text{NH}_4^+$ , and  $\text{Cl}^-$ , and  $\text{NO}_3^-$  was mainly anthropogenic origin.  $\text{NO}_3^-$  has shown an obviously positive correlation with  $\text{NH}_4^+$ ,  $\text{Cl}^-$ ,  $\text{Ca}^{2+}$ , and  $\text{K}^+$  ( $r > 0.5$ ) and a weak positive correlation with TDS (Table 3), indicating the contribution of atmospheric and anthropogenic sources, While the weak negative correlation between the couple ions of  $\text{Mg}-\text{Li}$ ,  $\text{Mg}-\text{Na}$ ,  $\text{SO}_4-\text{Mg}$ ,  $\text{HCO}_3-\text{Mg}$ , and  $\text{TDS}-\text{Mg}$

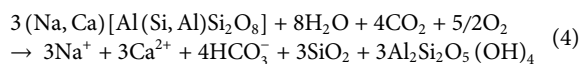
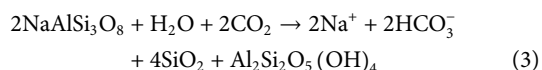
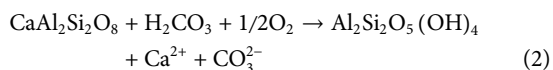
TABLE 3 Correlation coefficient (*r*) of chemical components of the water samples.

	Li <sup>+</sup>	Na <sup>+</sup>	NH <sub>4</sub> <sup>+</sup>	K <sup>+</sup>	Mg <sup>2+</sup>	Ca <sup>2+</sup>	F <sup>-</sup>	Cl <sup>-</sup>	NO <sub>3</sub> <sup>-</sup>	SO <sub>4</sub> <sup>2-</sup>	HCO <sub>3</sub> <sup>-</sup>	TDS
Li <sup>+</sup>	1											
Na <sup>+</sup>	0.9936	1										
NH <sub>4</sub> <sup>+</sup>	0.7984	0.8227	1									
K <sup>+</sup>	0.9157	0.9390	0.9112	1								
Mg <sup>2+</sup>	-0.2887	-0.2589	0.0544	-0.0504	1							
Ca <sup>2+</sup>	0.2976	0.3527	0.6378	0.5139	0.5644	1						
F <sup>-</sup>	0.8885	0.8784	0.6884	0.7909	-0.3739	0.3134	1					
Cl <sup>-</sup>	0.8199	0.8467	0.8677	0.8654	0.0894	0.7310	0.7802	1				
NO <sub>3</sub> <sup>-</sup>	0.3756	0.4200	0.6027	0.5065	0.3748	0.5490	0.1018	0.6171	1			
SO <sub>4</sub> <sup>2-</sup>	0.7921	0.7978	0.6969	0.7531	-0.2884	0.4982	0.9334	0.8159	0.1103	1		
HCO <sub>3</sub> <sup>-</sup>	0.9288	0.9517	0.8197	0.9361	-0.1075	0.3734	0.7211	0.7880	0.5487	0.6158	1	
TDS	0.9659	0.9840	0.8762	0.9600	-0.1488	0.5075	0.8740	0.9162	0.4867	0.8369	0.9405	1

(Table 3) may reflect water–rock interaction (dissolution, ion exchange and deposition).

In the diagram of Na–Mg–Cl concentrations (Figure 3), the data of water samples from the AVR scatter far from the marine precipitation lines (Keene et al., 1986) and show evidently different slopes, indicating the contribution of those ions from marine origin is negligible. The lines of Cl–Na and Cl–TDS in the water samples and solutions leaching granodiorite at ambient conditions (Du et al., 2010) have similar slopes and intersections, while those of Na–Mg are different. TDS, Cl, and Na in the samples are much higher than those in the leaching solutions (Figure 3), which indicate the ions mainly originate from Na–Cl-enriched deep geothermal fluids and the dissolution of Na-bearing minerals.

Plagioclase is a main component of the granite, granodiorite, and andesitic basalts that are widely distributed in the AVR (Figure 1). Na and Ca cations can be dissolved into solution through the reactions between plagioclase and CO<sub>2</sub>-bearing water.



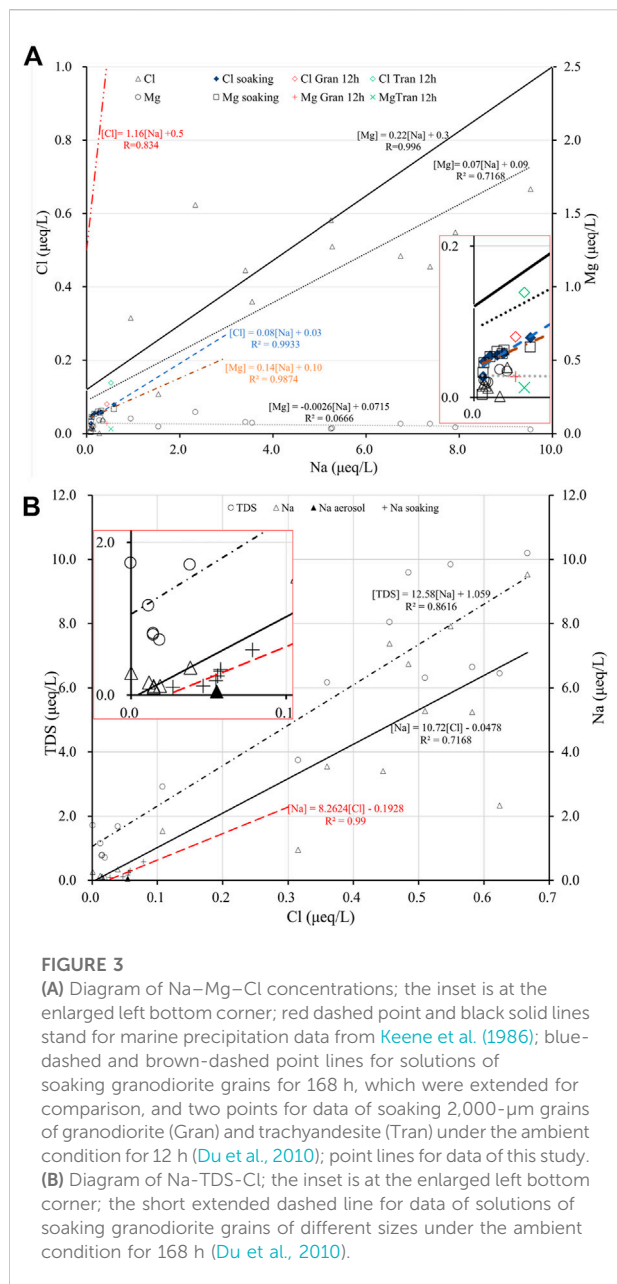
The decomposition reactions of plagioclase can be promoted by an increase in temperature, CO<sub>2</sub> partial pressure, and a mixture of Cl–S-enriched deep-earth fluids.

The Mg/Na and K/Na ratios of the rain and surface water samples from the AVR are concordant with those of marine precipitation (Keene et al., 1986) and water-soluble ions (Mg/Na=0.6 and K/Na=0.4) in aerosol samples in NE China (Shen

et al., 2007). This indicates that the ions in the rain sample and the surface waters are mainly derived from sources of continental aerosol, sea salt, and rock dissolution.

The Cl<sup>-</sup> concentrations of the rain and surface water samples are much lower than those of the hot spring waters, except for the sample AW-14 (Table 1; Figure 3), indicating the contribution of atmospheric and anthropogenic Cl to the hot spring waters is neglectable. Additionally, the values of Cl<sup>-</sup> and Na<sup>+</sup> concentrations and Mg/Na, Cl/Na, and Cl/Mg ratios of rock solutions differ from those of the hot spring water samples (Figure 3). The Na<sup>+</sup> concentration in the solution is about 2 magnitudes higher than Cl<sup>-</sup> concentration if granitic and andesitic rocks are dissolved in equal proportion. The experiments of soaking basalt and trachyandesite grains display that concentrations of Cl<sup>-</sup>, SO<sub>4</sub><sup>2-</sup>, and Na<sup>+</sup> approach the highest values in short time, and then, the highest value of Cl<sup>-</sup> of about 3 mg/L show no obvious variation with increasing soaking time, while others varied with soaking time (Du et al., 2010). Similarly, the observed and experimental results indicated that the meteoric waters picked up chloride more rapidly than they would be congruent dissolution of basalts, resulting in Cl<sup>-</sup> of 1–5 mg/L in the spring water (Gislason and Hans, 1987; Gislason et al., 1993). Such data indicate that the amount of Cl<sup>-</sup> in groundwater contributed by meteoric water dissolving igneous rocks ranges from 2 to 4 mg/L. Therefore, the ions in the hot spring water could be a mixture of rock solution and deep-earth fluids.

Cl<sup>-</sup> percentages of dissolution of rock and deep-earth fluids in the hot spring waters can be estimated by the two-member linear mixing model (Figure 4). Assuming Cl<sup>-</sup> concentration of the end member of dissolution of rock be 3 mg/L (Gislason and Hans, 1987; Du et al., 2010) and that of the end member of deep-earth fluids be 20,000 mg/L (Oita deep geothermal water Cl: 18,649–23,787 mg/L and Na: 12,213–15,813 mg/L (Amita et al., 2005)), the volume percentages of deep-earth fluids in the AVR



hot spring waters were estimated in the range from 0.041 to 0.103; in other words, 73%–87% of  $\text{Cl}^-$  in the hot spring waters were derived from deep-earth fluids. Moreover, taking the  $\text{Na}^+$  concentration of 3 mg/L in the 168-h soaking solution (Du et al., 2010) as the end member of dissolution of igneous rocks and that of 13,000 mg/L in Oita deep-earth fluids as another, the volume percentages of deep-earth fluids in the spring waters were estimated in the range of 0.14–1.66; that is, 86%–99% of  $\text{Na}^+$  in the hot spring waters were derived from deep-earth fluids (Table 1). Obviously, less than 1 vol% of deep-earth fluids mixed in the hot spring waters can be ignored when assessing groundwater volume, but the contributions of ions and heat

energy from the deep-earth fluids to the geothermal system are significant.

## 5.2 Origins of gases

### 5.2.1 Molecular compositions of the hot spring gases

The measured N–He–Ar abundance system in AVR obviously differs from the gaseous components in air-saturated water (ASW) (Table 2). The ratios of  $\text{N}_2/\text{O}_2$  and Ar/ $\text{O}_2$  of the samples are 44–67 and 0.07–1.11, respectively, except for 137.6 and 3.1 of the gas samples from the hot springs in JJG, which obviously differ from those of air (3.7 and 0.04) and those in ASW (1.81 and 0.03 (Weiss, 1970)). The  $\text{N}_2/\text{He}$  ratios of the gas samples range from 116.4 to 663.0, obviously differing from the atmospheric (15,000) and ASW values (11,400 (Weiss, 1970; Taran, 2011)). He concentrations in the gas samples are approximately 4 magnitudes larger than the atmospheric value, but the  $\text{N}_2/\text{He}$  ratios are about 2 magnitudes lower than ASW's value, and the  $^4\text{He}/^{20}\text{Ne}$  ratios of 257.8–385.3 of the hot spring gases are much higher than the atmospheric value (0.318 (Porcelli et al., 2002)) and ASW's value (0.222 at 3°C (Weiss, 1971)). The disparities of molecular parameters between the samples and air or ASW likely indicate that amounts of atmospheric  $\text{N}_2$  and He carried by meteoric water to the hot spring gases are not significant.

Sources of gases can be illustrated by the He–Ar– $\text{N}_2$  ternary diagram (Giggenbach et al., 1993; Rizzo et al., 2019; Bini et al., 2022).  $\text{O}_2$  and Ar in hot springs are often considered to be derived from air based on the fact that  $\text{O}_2$  and Ar concentrations in the atmosphere are much higher than those in the lithosphere, and hot spring water is mainly derived from meteoric water. In the case where all gaseous components in underground water originate from air, a part or all of the oxygen consumed by microbe respiration and the oxidation of organic and inorganic matter in the water circuit may result in  $\text{N}_2$ -rich gas. The low  $\text{CO}_2$  concentrations in the gas samples indicate that the  $\text{O}_2$  consumption of microbe respiration and the oxidation of organic matter in the hydrological circuit are neglectable. Data of our two gas samples are plotted nearby a magmatic source in the He–Ar– $\text{N}_2$  ternary diagram (Figure 5, Taran, 2011), indicating the gaseous components mainly originate from deep-earth fluids (Benavente et al., 2016). The data of the same hot springs obtained at different times (Zhao et al., 2021) shift to the air source in Figure 5, probably hinting at temporal variation or air contamination. The excess  $\text{N}_2$  ( $\text{N}_2^*$ ), Ar ( $\text{Ar}^*$ ), and amount of non-atmospheric components can be estimated using the concentration of  $\text{N}_2/\text{O}_2$  and Ar/ $\text{O}_2$  ratios of ASW (Taran, 2009). Assuming the measured  $\text{O}_2$  is derived from air and without consideration of  $\text{O}_2$  consume in the hydrological circuit,  $\text{Ar}^*$  can be estimated by  $\text{Ar}^* = (\text{Ar}/\text{O}_2 - 20.5)/\text{Ar}$ , and excess  $\text{N}_2$  can be estimated by  $\text{N}_2^* = (\text{N}_2 -$

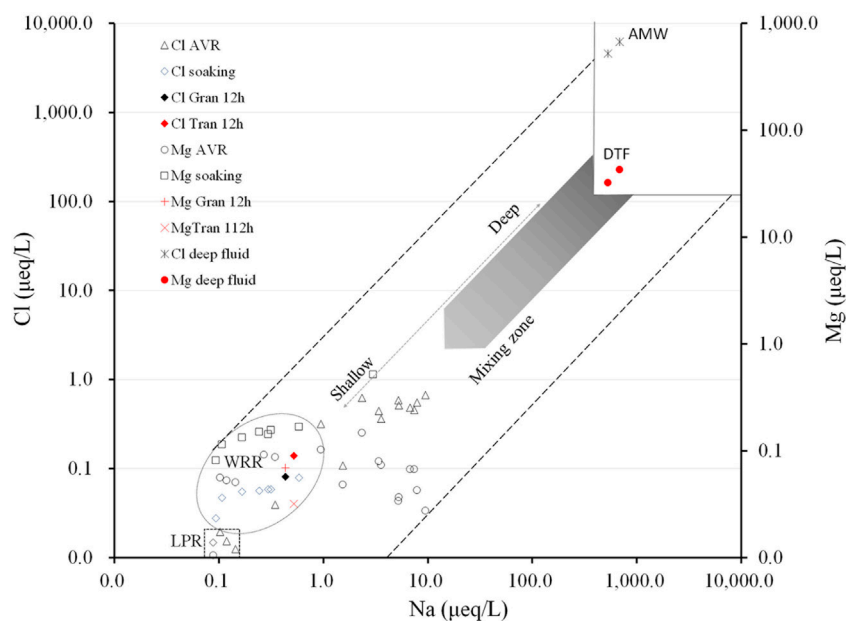


**FIGURE 4**

Source partitioning of Na–Mg–Cl ions in the AVR waters; data of deep-earth fluid after [Amita et al. \(2005\)](#); CI AVR and Mg AVR are in this study; others (solutions of soaking granodiorite and trachyandesite) are after [Du et al. \(2010\)](#); LPR is the local precipitation region (rectangle); WRR is the water–rock reaction region (oval); DTR is the deep-earth fluid region; AMW displays approximately andesitic-magmatic water.

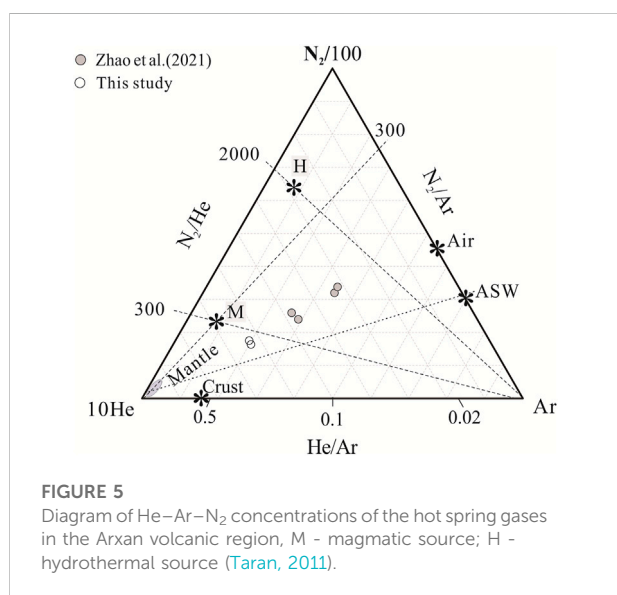


**FIGURE 5**

Diagram of He–Ar–N<sub>2</sub> concentrations of the hot spring gases in the Arxan volcanic region, M - magmatic source; H - hydrothermal source ([Taran, 2011](#)).

1.814 O<sub>2</sub>)/N<sub>2</sub> ([Table 2](#)). The calculated results indicated that more than 95% of N<sub>2</sub> and more than 91% of Ar in the gas samples were of no-atmospheric origin ([Table 2](#)). N<sub>2</sub>\*/Ar\* ratios ranged from 52.21 to 88.04, less than those of geothermal gases in the volcanic arc (107–388 ([Rouilleau et al., 2015](#))) and mantle (350 ([Taran, 2011](#))). The low N<sub>2</sub>\*/Ar\* ratios can be attributed to the contribution of radiogenic Ar produced by <sup>40</sup>K that is relatively

enriched in the granodiorite and alkaline basaltic rocks ([Figure 1](#)). Higher concentration He can be attributed to mantle-derived He and radiogenic He produced by the U–Th series enriched in the granodiorite and acid-intermediate volcanic rock in the crust.

## 5.2.2 Isotopic ratios of helium, carbon, and neon

### 5.2.2.1 He

In most cases, helium in geothermal fluids originates from atmospheric, crustal, and mantle sources ([Sano et al., 1985](#); [Ballentine et al., 2002](#); [Zhou et al., 2015](#); [Bini et al., 2022](#)). Several methods were proposed for source partitioning of He in geothermal gases. For example, [Sano et al. \(1985\)](#) used an equation set to calculate the He percentages of atmospheric, crust, and mantle sources on the basis of the given <sup>3</sup>He/<sup>4</sup>He and <sup>20</sup>Ne/<sup>4</sup>He ratios of those sources. Using a plot of CO<sub>2</sub>/<sup>3</sup>He vs. δ<sup>13</sup>C with the given values of the same parameters for the atmospheric, crust, and mantle sources, the source partitioning of He and CO<sub>2</sub> in the geothermal gases can be illustrated ([Sano and Marty, 1995](#); [Hilton, 1996](#)). Using the corrected <sup>3</sup>He/<sup>4</sup>He ratios deduced for atmospheric He by the <sup>4</sup>He/<sup>20</sup>Ne ratio of air or ASW, the non-atmospheric He can be estimated by the two-end member model of crust and mantle sources ([Ballentine et al., 2002](#); [Zhou et al., 2015](#)).

The samples of gases in the hot springs in AVR are characterized by low <sup>3</sup>He/<sup>4</sup>He and CO<sub>2</sub>/<sup>3</sup>He ratios ([Table 2](#)), which obviously differ from those of hydrothermal fluids in the

Wudalianchi volcanic area (low  $^3\text{He}/^4\text{He}$  and high  $\text{CO}_2/{}^3\text{He}$ ) in the rift valley (Du et al., 1999; Xu et al., 2013) and Tianchi volcanic area (high  $^3\text{He}/^4\text{He}$  and low  $\text{CO}_2/{}^3\text{He}$ ) neighboring the rift valley to the west in NE China (Shangquan et al., 1996), and much less than those of volcanic and geothermal gases in the volcanic arc and middle ocean ridge (Sano and Marty, 1995; Shaw et al., 2003). The  $^4\text{He}/^{20}\text{Ne}$  ratios of the gas samples are in the range of 0.34–385.3, and  $^4\text{He}$  concentrations and  $^3\text{He}/^4\text{He}$  ratios of the spring gases are independent (Table 2). The  $\text{CO}_2/{}^3\text{He}$  ratios of the gas samples are 3 magnitudes less than those of the mantle (MORB-type) ( $1.5 \times 10^9$  (Sano and Marty, 1995)), 3–5 magnitudes less than the values of fumaroles and hot springs in the volcanic areas in Japan ( $7.74 \times 10^9$ – $1.18 \times 10^{11}$  (Sano and Marty, 1995)) and in the Nicaraguan volcanic front (Shaw et al., 2003), and 8 magnitudes less than the values of sediment and limestone ( $1 \times 10^{13}$  (Sano and Marty, 1995; Xu et al., 2013)). Therefore, it can be concluded that that He in the gas samples has multiple origins.

The  $^{20}\text{Ne}/^{22}\text{Ne}$  ratios of the gas samples are close to the atmospheric value, and the  $^{21}\text{Ne}/^{22}\text{Ne}$  ratios are slightly less than the atmospheric value (Table 2), indicating that Ne is mainly derived from air. Assuming all the  $^{20}\text{Ne}$  in the geothermal gases is derived from air, the measured  $^3\text{He}/^4\text{He}$  ratios of geothermal gases can be corrected by  $^4\text{He}/^{20}\text{Ne}$  ratios of air or air-saturated water (Hilton, 1996; Ballentine et al., 2002; Xu et al., 2013; Zhou et al., 2015; Zhao et al., 2021). For eliminating the air contribution resulted from air dissolved in meteoric water into groundwater, the measured  $^3\text{He}/^4\text{He}$  ratios were corrected by the ASW's  $^4\text{He}/^{20}\text{Ne}$  ratio using the equation,  $(^3\text{He}/^4\text{He})^* = \{(^3\text{He}/^4\text{He})_{\text{sample}} - r\} / (1 - r)$ , where  $r = (^4\text{He}/^{20}\text{Ne})_{(\text{air or ASW})} / (^4\text{He}/^{20}\text{Ne})_{\text{sample}}$  (Xu et al., 2013). ASW's  $^4\text{He}/^{20}\text{Ne}$  ratio was calculated using the data of He and Ne solubility in water at 3 °C ( $4.814 \times 10^{-5}$  ml/kg and  $21.71 \times 10^{-5}$  ml/kg (Weiss, 1971)), and  $^{20}\text{Ne}$  content is 90.48% of total Ne (Porcelli et al., 2002), regardless of isotopic fractionations of He and Ne caused by air dissolution. The corrected  $^3\text{He}/^4\text{He}$  ratios of the gas samples from the Tianchi, JIG Tianchi crater lakes, the Budonghe water, and spring no. 0 differ evidently from the measured ratios, but those of the hot spring gas samples with high  $^4\text{He}/^{20}\text{Ne}$  ratios and high He concentrations show no change (Table 2). The percentages of atmospheric He and non-atmospheric He in the gas samples can be calculated by the following equation:

$$\frac{^3\text{He}}{^4\text{He}} = \text{Atm} \left( \frac{^3\text{He}}{^4\text{He}} \right)_a + (1 - \text{Atm}) \left( \frac{^3\text{He}}{^4\text{He}} \right)^*, \quad (5)$$

where  $(^3\text{He}/^4\text{He})$  is the measured value;  $\text{Atm}$  is the percentage of atmospheric He,  $(^3\text{He}/^4\text{He})_a$  is the atmospheric ratio; and  $(^3\text{He}/^4\text{He})^*$  is the ASW-corrected ratio or non-atmospheric He. The calculation results show the percentages of atmospheric He ( $\text{Atm}$ ) in the hot spring gases are less than 73, and those of non-atmospheric He range from 27 to 100 (Figure 6; Table 2).

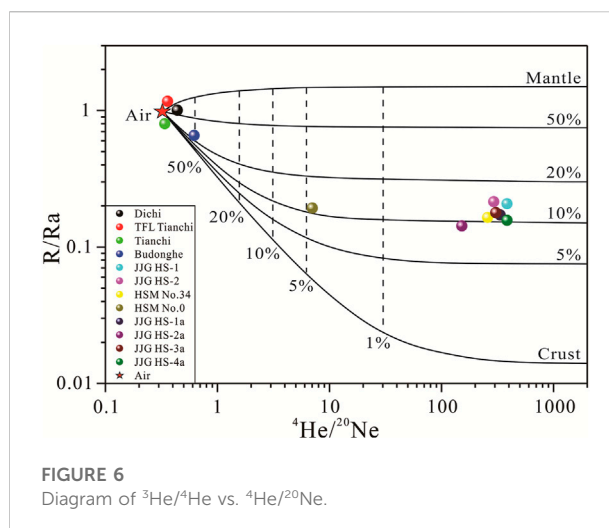


FIGURE 6  
Diagram of  $^3\text{He}/^4\text{He}$  vs.  $^4\text{He}/^{20}\text{Ne}$ .

Helium derived from the crustal and mantle origins can be quantitatively estimated by the two-member mixing model using the ASW (or air)-corrected  $^3\text{He}/^4\text{He}$  ratios (Ballentine et al., 2002; Zhou et al., 2015; Seki et al., 2019; Zhao et al., 2021). Traditionally, assuming the mantle be homogenous, the  $^3\text{He}/^4\text{He}$  ratios of the mantle and crust sources were proposed to be  $8 \pm 1 R_A$  and  $0.02 R_A$ , respectively (Sano and Marty, 1995). However, the chemical heterogeneity of the upper mantle must be emphasized to estimate the amount of mantle-derived He in the hot spring gas, which is involved in assessing heat flux and potential heat resources in the geothermal fields. The  $^3\text{He}/^4\text{He}$  ratios of basalts and mantle xenoliths in the different tectonic regions such as the mid-ocean ridge, volcanic arc, subcontinent, and orogenic zone evidently differ from each other and vary in a wide region within the same tectonic unit (Graham, 2002; Porcelli et al., 2002; Xu and Liu, 2002; Zhao et al., 2021; Randazzo et al., 2022). The  $^3\text{He}/^4\text{He}$  ratio for the European subcontinental lithospheric mantle source was proposed as  $6.1 \pm 0.9 R_A$  (Randazzo et al., 2022). The isotopic compositions of noble gases in mantle peridotite xenoliths in eastern China vary from place to place and are obviously lower than MORB values (Cui et al., 2022). The lithospheric mantle and the asthenosphere in the continent area are important sources of gases in the upper mantle, which differs from the orogenic ranges to the rift valley in NE China (Xu et al., 2013). The mantle peridotite xenoliths in the Arxan–Chahe region (Liu et al., 2001; Sui et al., 2012) are geochemically similar to those in the Hannuoba region (Song and Frey, 1989; E and Zhao, 1987). Both the Arxan and Hannuoba volcanic regions are located in the orogenic belt of the Greater Khingan Range–Taihang Mountains, neighboring the rift valley on the east. The alkali basalts in the two regions formed in Miocene–Holocene, of which the REE patterns and spiderweb diagrams are similar (Zhao, 2010). The mantle xenoliths found in the two regions are mainly Al-rich lherzolites (E and Zhao, 1987). Therefore, the upper mantle from

the Hannuoba region to the south part of the Greater Khingan Range can be considered the same, implying that there is no obvious difference between the mantle sources of He in both the AVR and Hannuoba region in the Cenozoic Era. Therefore,  $^3\text{He}/^4\text{He}$  of the mantle source in the AVR can be represented by the average ( $2.1 \times 10^{-6}$ ) of  $^3\text{He}/^4\text{He}$  ( $n=31$ ) of mantle peridotite xenoliths in the Hannuoba region (Cui et al., 2022). On the assumption that the  $^3\text{He}/^4\text{He}$  ratios of the crustal and upper mantle sources are  $2 \times 10^{-8}$  and  $2.1 \times 10^{-6}$ , respectively, contributions of mantle-derived He to the total He of the hot spring gases were estimated in a range of 3%–23% using the ASW-corrected  $^3\text{He}/^4\text{He}$  ratios and percentages of non-atmospheric He in the total He and percentages of crustal He range from 9 to 94 (Table 2). Source partitioning can be illustrated by the diagram of  $^3\text{He}/^4\text{He}$  vs.  $^4\text{He}/^{20}\text{Ne}$  (Figure 6). The percentages of mantle-derived He in the high-temperature spring gases in Figure 6 are slightly higher than the calculated values (Table 2). In consideration of the uncertainty of the different methods, however, it is clear that the calculated results are in general comparable with the diagram of  $^3\text{He}/^4\text{He}$  vs.  $^4\text{He}/^{20}\text{Ne}$  (Figure 6). He percentages of the primary mantle source in the gas samples range from 1% to 6%, estimated with the MORB value (Table 2). The bubble gas in the Tuofenglin crater lake has the highest percentage of mantle He and is composed of 68% of atmospheric He, 23% of mantle He, and 9% of crustal He. The high percentages of mantle He are found in the crater lakes (Figure 1), indicating that the mantle He migrates upwards to the surface through fractures in the channel of magma migration and mixes with atmospheric and crustal He during migration. The contribution of atmospheric He to the gases in the high-temperature hot springs in the Jinjiangou area is negligible. Gas in the low-temperature spring of no. 0 around the Hot Spring Museum (Figure 1B) contains about 3% of atmospheric He, but gas in the high-temperature hot spring on no. 34 lack of atmospheric He (Table 2; Figure 6). Such a small amount of atmospheric He may be carried into the spring by cool water recharge containing dissolved atmospheric He. Specially, the amount of mantle-derived He in the Budonghe water was estimated as high as 12%, which indicated that plenty of heat energy was transported by deep-earth fluids from the upper mantle to the Budonghe area in the Wuliqiao geothermal field. He in the hot spring gases with high concentrations is predominantly of crust origin, with less than 10% of mantle-derived He, indicating He accumulation in the geothermal reservoirs. The mantle-derived He emits upwards to the surface through the deep-cut faults and transports plenty of heat energy to the geothermal systems, which is supported by the data that about 80% of total heat flow is derived from the mantle in the study area (Sun, 1999).

#### 5.2.2.2 CO<sub>2</sub>

Concentrations of CO<sub>2</sub> in the hot spring gases in the AVR are less than 1%, and  $\delta^{13}\text{C}$  values are in the range of  $-15.9$ – $-22.3$ %

(Table 2). There are three scenarios for the origin of CO<sub>2</sub> in the spring gases in the AVR. The first one is that CO<sub>2</sub> in the hot springs is likely derived from the mantle based on the mean value of  $-22.6$ % ( $n = 105$ ) of CO<sub>2</sub> in mantle xenoliths and minerals enclosed in Cenozoic basalts in eastern China (Cui et al., 2022). The statistical result of the  $\delta^{13}\text{C}$  values of CO<sub>2</sub> in the mantle xenoliths worldwide also shows a bimodal distribution with peak values of  $-5$ % and  $-25$ % (Deines, 2002). The second one is that the CO<sub>2</sub> is likely to have originated from biogenic and metamorphic gases in the crust. The  $\delta^{13}\text{C}$  values of CO<sub>2</sub> originating from Jurassic coal seams are in a range of  $-11$ %– $-28$ % (Du and Liu, 1991). Biogenic CO<sub>2</sub> of concentrations less than 6% in the gas reservoirs and gas seepages in China has  $\delta^{13}\text{C}$  values between  $-10$ % and  $-22$ % (Dai et al., 1996). The third one is that the CO<sub>2</sub> is most likely a mixture of biogenic and abiogenic CO<sub>2</sub>.  $\delta^{13}\text{C}$  data ( $-4.7$ %– $-6.4$ %) of CO<sub>2</sub> in the fumarolic gases at the Longonot Volcano, Kenya, indicated a magmatic origin with minor contributions from biogenic CO<sub>2</sub> (Robertson et al., 2016).

#### 5.2.2.3 N<sub>2</sub>

Nitrogen, in some instances, is the main component in hot spring, fumarole, and volcanic gases, which were identified as a mixture of atmospheric, mantle, and crustal N<sub>2</sub> (Rouilleau et al., 2015; Tardani et al., 2016; Zhao et al., 2021). N<sub>2</sub> is the predominant component in the hot spring gases in the AVR, and  $\delta^{15}\text{N}$  values are in a range of  $+1.3$ – $+1.9$ % (Table 2). The excess N<sub>2</sub> content is larger than 92%. Combining with  $^4\text{He}/^{20}\text{Ne}$  and  $^3\text{He}/^4\text{He}$  ratios and the lack of organic matter to produce lot of metamorphic nitrogen in the study area, it can be considered that the excess N<sub>2</sub> mainly originated from the mantle with mixing crust-derived N<sub>2</sub>, as reported by Zhao et al. (2021).

## 6 Conclusion

The origins of the spring water and gases in the AVR were traced by the hydro- and gas-chemical data. Contributions of deep-earth fluids to the geothermal systems were estimated using Cl<sup>-</sup> and Na<sup>+</sup> concentrations, ASW-corrected  $^3\text{He}/^4\text{He}$  ratios, and the regional mantle helium isotope ratio in consideration of the heterogeneity of the upper mantle. The conclusions are remarked as follows:

- 1 H<sub>2</sub>O in the river, lakes, and spring waters predominantly originate from meteoric water. The small amount (<1%) of H<sub>2</sub>O derived from deep-earth fluids seems negligible for assessing the volume of geothermal fluid, but the ion contributions of deep-earth fluids to the hot spring water are significant. Ions in the rain sample were mainly derived from sea salt and continental aerosol. Ions in the surface waters have multiple sources of the continental aerosol, sea salt, rock dissolution, and anthropogenic sources, while ions in the hot spring waters are

predominantly derived from deep-earth fluids. That 73%–87% of  $\text{Cl}^-$  and 86%–99% of  $\text{Na}^+$  in the hot spring waters may be derived from deep-earth fluids.

2 Enrichment of heavy isotopes in the rainwater can be attributed to isotopic fractionation caused by raindrop evaporation. Heavier isotope compositions of the waters in the crater lakes may be caused by the evaporation process due to the higher evaporation capacity in the study area.

3 Atmospheric neon dissolution in the lake waters likely approached the balance state.  $\text{CH}_4$  in the hot springs isotopically displays a biogenic origin. Excess  $\text{N}_2$ , Ar, and  $\text{CO}_2$  in the hot spring gases could be predominantly derived from both the crust and upper mantle sources.

4 Contributions of the mantle-derived He to bubble gases in the hot spring were estimated in a range of 3%–23%. High percentages of mantle-derived He in the bubbling gases in the crater lakes indicate gases in the mantle emit upwards through the channel for magma migration; 12% of the total He of dissolved gas in the Budonghe water is derived from the mantle, indicating deep-earth fluids transport continuously plenty of heat to the Budonghe and the geothermal systems.

## Data availability statement

The original contributions presented in the study are included in the article/Supplementary Material; further inquiries can be directed to the corresponding authors.

## Author contributions

YC, LL, CX, JL, ZC, and JD conducted the field survey. YC and JD processed the data and prepared the first draft. All co-authors edited the manuscript.

## References

- Amita, K., Ohsawa, S., Du, J., and Yamada, M. (2005). Origin of Arima-type deep thermal water from hot spring wells in Oita Plain, eastern Kyushu, Japan. *Hot Spring Sci.* 55 (2), 64–77. (in Japanese with English abstract).
- Bai, Z., Tian, M., and Wu, F. (2005). Yanshan, gaoshan: Two active volcanoes of the volcanic cluster in arxan, inner Mongolia. *Earthq. Res. China* 21 (1), 113–117. (In Chinese with English abstract).
- Ballentine, C. J., Burgess, R., and Marty, B. (2002). “Tracing fluid origin, transport and interaction in the crust,” in *Mineralogy and Geochemistry* 47 (1), 539–614. doi:10.2138/rmg.2002.47.13
- Barry, P. H., Negrete-Aranda, R., Spelz, R. M., Seltzer, A. M., Bekaert, D. V., Virrueta, C., et al. (2020). Volatile sources, sinks and pathways: A helium-carbon isotope study of baja California fluids and gases. *Chem. Geol.* 550, 119722. doi:10.1016/j.chemgeo.2020.119722
- Benavente, O., Tassi, F., Reich, M., Aguilera, F., Capecciacci, F., Gutiérrez, F., et al. (2016). Chemical and isotopic features of cold and thermal fluids discharged in the Southern Volcanic Zone between 32.5°S and 36°S: Insights into the physical and chemical processes controlling fluid geochemistry in geothermal systems of Central Chile. *Chem. Geol.* 420, 97–113. doi:10.1016/j.chemgeo.2015.11.010
- Bini, G., Chiodini, G., Caliro, S., Tassi, F., Vaselli, O., Rizzo, A. L., et al. (2022). Nitrogen, helium, and argon reveal the magmatic signature of fumarole gases and episodes of outgassing from upper-crustal magma reservoirs: The case of the Nisyros caldera (Aegean Arc, Greece). *Geochim. Cosmochim. Acta* 335, 68–84. doi:10.1016/j.gca.2022.08.028
- Chen, J., Wang, W., and Ma, F. (2021). Recharge source and Genesis analysis of Cenozoic basalt groundwater in Arshan. *J. Hohai Univ. Nat. Sci.* 49 (3), 249–256. (In Chinese with English abstract). doi:10.3876/j.issn.1000-1980.2021.03.007
- Chen, Z., Du, J., Zhou, X., Yi, L., Liu, L., Xie, C., et al. (2014). Hydrochemistry of the hot springs in Western Sichuan province related to the Wenchuan  $M_s$  8.0 earthquake. *Sci. World J.* 2014 (1), 1–13. doi:10.1155/2014/901432
- Cui, Y., Sun, F., and Du, J. (2022). Methods for identification of seismic geochemical precursors and source partitioning of hot spring fluids in Eastern Chinese Mainland. *J. Seismol. Res.* 45 (2), 199–216. (In Chinese with English abstract). doi:10.20015/j.cnki.ISSN1000-0666.2022.0053
- Dai, J., Song, Y., and Da, C. (1996). Geochemistry and accumulation of carbon dioxide gases in China. *Am. Assoc. Pet. Geol. Bull.* 80, 1615–1626. doi:10.1306/64EDA0D2-1724-11D7-8645000102C1865D

## Funding

This work was supported by the National Key Research and Development Program (2019YFC1509203), the Open Foundation of the United Laboratory of High Pressure Physics and Earthquake Science (2019HPPES08), and the National Natural Science Foundation of China (41403099).

## Acknowledgments

The authors are grateful to Ruijie Zhang in the Arxan Observatory of Volcano for his help in the field trip and Zhaofei Liu and Jianan Huang for drawing the figures. They are extremely grateful to the four reviewers for their constructive comments and patience during discussion.

## Conflict of interest

The authors declare that the research was conducted in the absence of any commercial or financial relationships that could be construed as a potential conflict of interest.

The handling editor MZ declared a past co-authorship with the author YL.

## Publisher's note

All claims expressed in this article are solely those of the authors and do not necessarily represent those of their affiliated organizations, or those of the publisher, the editors, and the reviewers. Any product that may be evaluated in this article, or claim that may be made by its manufacturer, is not guaranteed or endorsed by the publisher.

- Deines, P. (2002). The carbon isotope geochemistry of mantle xenoliths. *Earth Sci. Rev.* 58 (3–4), 247–278. doi:10.1016/S0012-8252(02)00064-8
- Du, J., Amida, K., Ohsawa, S., Zhang, Y., Kang, C., and Yamada, M. (2010). Experimental evidence on imminent and short-term hydrochemical precursors for earthquake. *App. Geochem.* 25, 586–592. doi:10.1016/j.apgeochem.2010.01.015
- Du, J., Cheng, W., Zhang, Y., Jian, C., Guan, Z., Liu, W., et al. (2006). Helium and carbon isotopic compositions of thermal springs in the earthquake zone of Sichuan, Southwestern China. *J. Asian Earth Sci.* 26, 533–539. doi:10.1016/j.jseas.2004.11.006
- Du, J., Li, S., Zhao, Y., Ren, J., Sun, R., and Duanmu, H. (1999). Geochemical characteristics of gases from the volcanic area Wudalianchi, Northeastern China. *Acta Geol. Sin.* 73 (2), 103–107. doi:10.1111/j.1755-6724.1999.tb00830.x
- Du, J., Liu, C., Fu, B., Zhang, Y., Wang, C., Wang, H., et al. (2005). Variations of geothermometry and chemical-isotopic compositions of hot spring fluids in the Rehai geothermal field, southwestern China. *J. Volcanol. Geotherm. Res.* 142 (3–4), 243–261. doi:10.1016/j.jvolgeores.2004.11.009
- Du, J., and Liu, W. (1991). Isotopic geochemistry of nonhydrocarbons in natural gas from sanshui basin, guangdong province. *Chin. J. Geochem.* 10 (4), 318–325. doi:10.1007/BF02841092
- Fan, Q., Zhao, Y., Li, D., Wu, Y., Sui, J., and Zheng, D. (2011). Studies on Quaternary volcanism stages of Halahe river and Chaoer river area in the Great Xing'an Range: Evidence from K-Ar dating and volcanic geology features. *Acta Pet. Sin.* 27 (10), 2827–2832.
- Fan, W., Guo, F., Wang, Y. J., and Lin, G. (2003). Late Mesozoic calc-alkaline volcanism of post-orogenic extension in the northern Da Hinggan Mountains, northeastern China. *J. Volcanol. Geotherm. Res.* 121 (1), 115–135. doi:10.1016/S0377-0273(02)00415-8
- Gao, H., Li, C., Sun, B., Shi, X., Zhao, S., and Fan, C. (2018). Characteristics of hydrogen and oxygen stable isotopes in Lake Hulun Basin and its indicative function in evaporation. *J. Lake Sci.* 30 (1), 211–219. doi:10.18307/2018.0121
- Giggenbach, W. F., Sano, Y., and Wakita, H. (1993). Isotopes of He, and CO<sub>2</sub> and CH<sub>4</sub> contents in gases produced along the New Zealand part of a convergent plate boundary. *Geochim. Cosmochim. Acta* 57, 3427–3455. doi:10.1016/0016-7037(93)90549-C
- Gislason, S. R., and Hans, P. E. (1987). Meteoric water-basalt interactions. I: A laboratory study. *Geochim. Cosmochim. Acta* 51 (10), 2827–2840. doi:10.1016/0016-7037(87)90161-X
- Gislason, S. R., Veblen, D. R., and Livi, K. J. T. (1993). Experimental meteoric water-basalt interactions: Characterization and interpretation of alteration products. *Geochim. Cosmochim. Acta* 57 (7), 1459–1471. doi:10.1016/0016-7037(93)90006-1
- Graham, D. W. (2002). “Noble gas isotope geochemistry of mid-ocean ridge and ocean island basalts: Characterization of mantle source reservoirs,” in *Mineralogy and Geochemistry* (1), 47, 247–318. doi:10.2138/rmg.2002.47.8
- Gu, X., Zhang, Q., Cui, Y., Shao, J., Xiao, Y., Zhang, P., et al. (2017). Hydrogeochemistry and genesis analysis of thermal and mineral springs in arxan, northeastern China. *Water* 9 (1), 61–17. doi:10.3390/w9010061
- Han, Z., Shi, X., Jia, K., Sun, B., Zhao, S., and Fu, C. (2019). Determining the discharge and recharge relationships between lake and groundwater in Lake Hulun using hydrogen and oxygen isotopes and chloride ions. *Water* 11 (2), 264. doi:10.3390/w11020264
- Hilton, D. R. (1996). The helium and carbon isotope systematics of a continental geothermal system: results from monitoring studies at Long Valley caldera (California, U.S.A.). *Chem. Geol.* 127, 269–295. doi:10.1016/0009-2541(95)00134-4
- Jia, Z., and Zhang, G. (2020). Teleseismic tomography for imaging the upper mantle beneath northeast China. *Appl. Sci. (Basel)*. 10 (13), 4557. doi:10.3390/app10134557
- Keene, W. C., Pszeny, A. A. P., Galloway, J. N., and Hawley, M. E. (1986). Seawater corrections and interpretation of constituent ratios in marine precipitation. *J. Geophys. Res.* 91 (D6), 6647. doi:10.1029/JD091iD06p06647
- Li, J. (2020). “Isotopic hydrochemical study of geothermal fluids in volcanic geothermal system.” M.A. thesis (Xi'an, China: Chang'an University). (In Chinese with English abstract).
- Li, X., Zhang, M., Ma, Q., Li, Y., Wang, S., and Wang, B. (2012). Characteristics of stable isotopes in precipitation over northeast China and its water vapor sources. *J. Env. Sci.* 33 (9), 2924–2931. (In Chinese with English abstract).
- Li, Y., Gao, R., Yao, Y., Mi, S., Li, W., Xiong, X., et al. (2014). The crust velocity structure of Da Hinggan Ling orogenic belt and the basins on both sides. *Prog. Geophys.* 29 (1), 315–341. doi:10.6038/pg20140110
- Li, Z., Tao, M., Li, L., Wang, Z., Du, L., and Zhang, M. (2007). Determination of isotope composition of dissolved inorganic carbon by gas chromatography-conventional isotope-ratio mass spectrometry. *Chin. J. Anal. Chem.* 35, 1455–1458. doi:10.1016/S1872-2040(07)60089-9
- Liang, L., Li, C., Shi, X., Sun, B., Wang, J., and Zhou, J. (2017). Characteristics of hydrogen and oxygen isotopes of surface and ground water and the analysis of source of Lake water in Hulun Lake. *Wetl. Sci.* 15 (3), 385–390. doi:10.13248/j.cnki.wetlandsci.2017.03.010
- Liu, J., Han, J., and Fyfe, W. S. (2001). Cenozoic episodic volcanism and continental rifting in northeast China and possible link to Japan Sea development as revealed from K-Ar geochronology. *Tectonophysics* 339, 385–401. doi:10.1016/S0040-1951(01)00132-9
- Liu, J., Song, X., Yuan, G., Sun, X., and Yang, L. (2014). Stable isotopic compositions of precipitation in China. *Tellus B Chem. Phys. Meteorology* 66 (1), 22567. doi:10.3402/tellusb.v66.22567
- Porcelli, D., Ballentine, C. J., and Wieler, R. (2002). “An overview of noble gas geochemistry and cosmochemistry,” in *Noble gases in Geochemistry and cosmochemistry*. Editors D. Porcelli, C. Ballentine, and R. Wieler. Rev. Mineral. Geochem. (Washington DC: Mineralogical Society of America), 47, 1–19.
- Qi, F., Zhang, F., Lu, S., and Sun, Y. (2012). The geothermal geological features of Arxan mountains. *Jinlin Geol.* 31 (2), 109–102. (In Chinese with English abstract).
- Randazzo, P., Caracausi, A., Aiuppa, A., Cardellini, C., Chiodini, G., Apollaro, C., et al. (2022). Active degassing of crustal CO<sub>2</sub> in areas of tectonic collision: A case study from the Pollino and Calabria sectors (Southern Italy). *Front. Earth Sci.* 10, 946707. doi:10.3389/feart.2022.946707
- Rizzo, A. L., Caracausi, A., Chavagnac, V., Nomikou, P., Polymenakou, P. N., Mandalakis, M., et al. (2019). Geochemistry of CO<sub>2</sub>-rich gases venting from submarine volcanism: The Case of Kolumbo (Hellenic Volcanic Arc, Greece). *Front. Earth Sci.* 7, 60. doi:10.3389/feart.2019.00060
- Robertson, E., Biggs, J., Edmonds, M., Clor, L., Fischer, T. P., Vye-Brown, C., et al. (2016). Diffuse degassing at Longonot volcano, Kenya: Implications for CO<sub>2</sub> flux in continental rifts. *J. Volcanol. Geotherm. Res.* 327, 208–222. doi:10.1016/j.jvolgeores.2016.06.016
- Roulleau, E., Vinet, N., Sano, Y., Takahata, N., Shinohara, H., Oooki, M., et al. (2015). Effect of the volcanic front migration on helium, nitrogen, argon, and carbon geochemistry of hydrothermal/magmatic fluids from Hokkaido volcanoes, Japan. *Chem. Geol.* 414, 42–58. doi:10.1016/j.chemgeo.2015.08.006
- Rozanski, K., Araguas-Araguas, L., and Gonfiantinni, R. (1993). “Isotopic patterns in modern global precipitation,” in *The climate change in continental isotopic records*. Editors P. K. Swart, K. C. Lohmann, and J. McKenzie (Washington, DC, USA: American Geophysical Union), 78, 1–36. doi:10.1029/GM078p0001
- Sano, Y., and Marty, B. (1995). Origin of carbon in fumarolic gas from island arcs. *Chem. Geol.* 119 (1–4), 265–274. doi:10.1016/0009-2541(94)00097-R
- Sano, Y., Nakamura, Y., and Wakita, H. (1985). Areal distribution of <sup>3</sup>He/<sup>4</sup>He ratios in the Tohoku district, Northeastern Japan. *Chem. Geol. Isot. Geosci. Sect.* 52 (1), 1–8. doi:10.1016/0168-9622(85)90004-1
- Seki, K., Ohba, T., Aoyama, S., Ueno, Y., Sumino, H., Kanda, W., et al. (2019). Variations in thermal state revealed by the geochemistry of fumarolic gases and hot-spring waters of the Tateyama volcanic hydrothermal system, Japan. *Bull. Volcanol.* 81, 8. doi:10.1007/s00445-018-1264-7
- Shangguan, Z., Kong, L., Sun, F., and Gao, S. (1996). Deep-seated fluid components and stable isotopic compositions in Tianchi volcanic area, Changbaishan Mountains. *Chin. J. Geol.* 31 (1), 54–64. (In Chinese with English abstract).
- Shaw, A. M., Hilton, D. R., Fischer, T. P., Walker, J., and Alvarado, G. (2003). Contrasting He-C relationships in Nicaragua and Costa Rica: insights into C cycling through subduction zones. *Earth Planet. Sci. Lett.* 214, 499–513. doi:10.1016/S0012-821X(03)00401-1
- Shen, Z., Cao, J., Arimoto, R., Zhang, R., Jie, D., Liu, S., et al. (2007). Chemical composition and source characterization of spring aerosol over Horqin sand land in northeastern China. *J. Geophys. Res.* 112, D14315. doi:10.1029/2006JD007991
- Sokolov, D. S. (1966). *Hydrogeology in U.S.S.R* (Moscow: Publishing House Nedra), 1, 432. (in Russian).
- Song, Y., and Frey, F. A. (1989). Geochemistry of peridotite xenoliths in basalt from Hannuoba, Eastern China: Implications for subcontinental mantle heterogeneity. *Geochim. Cosmochim. Acta* 53, 97–113. doi:10.1016/0016-7037(89)90276-7
- Sui, J., Fan, Q., and Xu, Y. (2012). Discovery of peridotite xenoliths from the Nuomin river Quaternary volcanic field, the Grea Xing'an Range, and its geological significance. *Acta petro. Sin.* 28 (4), 1130–1138.
- Sun, C. (1999). “Study of geothermal structure of hot springs in Arxan,” master's thesis (Changchun, China: Jilin University). (In Chinese with English abstract).
- Sun, Y., Guo, Z., and Fortin, D. (2020). Carbon dioxide emission from monogenetic volcanoes in the Mt. Changbai volcanic field, NE China. *Int. Geol. Rev.* 63 (14), 1803–1820. doi:10.1080/00206814.2020.1802782

- Tang, J., Wang, J., Chen, X., Zhao, G., and Zhan, Y. (2005). A Preliminary Investigation on Electric Structure of the Crust and Upper Mantle in Arxan Volcanic Area. *Chin. J. Geophys.* 48 (1), 214–221. doi:10.1002/cjg2.642
- Tang, S. (1984). Feature of the Late Jurassic volcanic structure and genetic mechanism of hot springs in Arxan. *Jilin Geol.* 38(1), 54–65. (In Chinese with English abstract).
- Taran, Y. A. (2009). Geochemistry of volcanic and hydrothermal fluids and volatile budget of the Kamchatka–Kuril subduction zone. *Geochim. Cosmochim. Acta* 73, 1067–1094. doi:10.1016/j.gca.2008.11.020
- Taran, Y. A. (2011). N<sub>2</sub>, Ar, and He as a tool for discriminating sources of volcanic fluids with application to Vulcano. *Bull. Volcanol.* 73 (4), 395–408. doi:10.1007/s00445-011-0448-1
- Tardani, D., Reich, M., Roulleau, E., Takahata, N., Sano, Y., Pérez-Flores, P., et al. (2016). Exploring the structural controls on helium, nitrogen and carbon isotope signatures in hydrothermal fluids along an intra-arc fault system. *Geochim. Cosmochim. Acta* 184, 193–211. doi:10.1016/j.gca.2016.04.031
- Tsujimura, M., Abe, Y., Tanaka, T., Shimada, J., Higuchi, S., Yamanaka, T., et al. (2007). Stable isotopic and geochemical characteristics of groundwater in Kherlen River basin, a semi-arid region in eastern Mongolia. *J. Hydrol. X.* 333 (1), 47–57. doi:10.1016/j.jhydrol.2006.07.026
- Wei, F., Xu, J., Shangguan, Z., Pan, B., Yu, H., Wei, W., et al. (2016). Helium and carbon isotopes in the hot springs of Changbaishan Volcano, northeastern China: A material connection between Changbaishan Volcano and the west Pacific plate? *J. Volcanol. Geotherm. Res.* 327, 398–406. doi:10.1016/j.jvolgeores.2016.09.005
- Weiss, R. F. (1971). Solubility of helium and neon in water and seawater. *J. Chem. Eng. Data* 16 (2), 235–241. doi:10.1021/je60049a019
- Weiss, R. F. (1970). The solubility of nitrogen, oxygen and argon in water and seawater. *Deep Sea Res. Oceanogr. Abstr.* 17 (4), 721–735. doi:10.1016/0011-7471(70)90037-9
- Xie, H., Tian, J., Wu, L., Zhu, Y., Wu, C., Shen, K., et al. (2011). Age of ore-forming granites in Aershan area of Inner Mongolia and its significance for prospecting. *J. Jilin Univ. (Earth Sci. Ed.)* 41 (5), 1432–1440.
- Xu, S., and Liu, C. (2002). Abundance and isotope ratios of noble gas in mantle xenoliths from northeastern China. *Chin. Sci. Bull.* 47 (2), 141–146. (In Chinese).
- Xu, S., Zheng, G., Nakai, S., Wakita, H., Wang, X., and Guo, Z. (2013). Hydrothermal He and CO<sub>2</sub> at Wudalianchi intra-plate volcano, NE China. *J. Asian Earth Sci.* 62, 526–530. doi:10.1016/j.jseae.2012.11.001
- Xue, X., Chen, L., Liu, J., He, Y., Wang, X., Zeng, G., et al. (2019). Primordial peridotitic mantle component in asthenosphere beneath Northeast China: Geochemical evidence from Cenozoic basalts of Greater Khingan Range. *Earth Sci.* 44 (4), 1143–1158. doi:10.3799/dqkx.2019.951
- Zhang, L., Chen, Z., Nie, Z., Liu, F., Jia, Y., and Zhang, X. (2008). Correlation between  $\delta^{18}\text{O}$  in precipitation and surface air temperature on different time-scale in China. *Nucl. Tech.* 31(9), 715–720. (In Chinese with English abstract).
- Zhang, P. (2017). “Hydrochemical characteristics and water rock interaction of Arxan Springs.” master’s theses (Beijing, China: China University of Geosciences).
- Zhang, W., Du, J., Zhou, X., and Wang, F. (2016). Mantle volatiles in spring gases in the Basin and Range Province on the west of Beijing, China: Constraints from helium and carbon isotopes. *J. Volcanol. Geotherm. Res.* 309, 45–52. doi:10.1016/j.jvolgeores.2015.10.024
- Zhao, D. (1987). *Cenozoic Basalts and Plutonic Inclusions in Eastern China*, Beijing, China: Science Press, 490. (In Chinese)
- Zhao, W., Guo, Z., Lei, M., Zhang, M., Ma, L., Fortin, D., et al. (2019). Volcanogenic CO<sub>2</sub> degassing in the Songliao continental rift system, NE China. *Geofluids* 2019, 1–14. doi:10.1155/2019/8053579
- Zhao, W., Guo, Z., Liu, J., Zhang, M., Sun, Y., Lei, M., et al. (2021). Fluxes and Genesis of carbon dioxide emissions from Cenozoic volcanic fields in NE China. *Ata Pet. Sin.* 37 (4), 1255–1269. doi:10.18654/1000-0569/2021.04.17
- Zhao, Y. (2010). dissertation. Beijing, China: Institute of Geology, China Earthquake Administration. Study on Geology and Geochemistry of Quaternary Volcanoes in the Da Hinggan Ling Mountains,
- Zhou, X., Wang, W., Chen, Z., Yi, L., Liu, L., Xie, C., et al. (2015). Gas geochemistry of hot springs in Western Sichuan Province, China after the Wenchuan M<sub>s</sub> 8.0 earthquake. *Terr. Atmos. Ocean. Sci.* 26 (4), 361–373. doi:10.3319/tao.2015.01.05.01(tt)